

# A Survey of Local Group Galaxies Currently Forming Stars: II. *UBVRI* Photometry of Stars in Seven Dwarfs and a Comparison of the Entire Sample

Philip Massey,<sup>1,2</sup> K. A. G. Olsen,<sup>3</sup> Paul W. Hodge,<sup>4</sup> George H. Jacoby,<sup>5</sup>  
Reagin T. McNeill,<sup>1,6</sup> R. C. Smith,<sup>3</sup> Shay B. Strong<sup>1,7</sup>

## ABSTRACT

We have obtained *UBVRI* images with the Kitt Peak and Cerro Tololo 4-m telescopes and Mosaic cameras of seven dwarfs in (or near) the Local Group, all of which have known evidence of recent star formation: IC10, NGC 6822, WLM, Sextans B, Sextans A, Pegasus, and Phoenix. We construct color-magnitude diagrams (CMDs) of these systems, as well as neighboring regions that can be used to evaluate the degree of foreground contamination by stars in the Milky Way. Inter-comparison of these CMDs with those of M31, M33, the LMC, and the SMC permits us to determine improved reddening values for a typical OB star found within these galaxies. All of the CMDs reveal a strong or modest number of blue supergiants. All but Pegasus and Phoenix also show the clear presence of red supergiants in the CMD, although IC10 appears to be deficient

---

<sup>1</sup>Lowell Observatory, 1400 W. Mars Hill Rd., Flagstaff, AZ 86001; Phil.Massey@lowell.edu.

<sup>2</sup>Visiting Astronomer, Kitt Peak National Observatory, National Optical Astronomy Observatory (NOAO), which is operated by the Association of Universities for Research in Astronomy (AURA), Inc., under cooperative agreement with the National Science Foundation (NSF).

<sup>3</sup>Cerro Tololo Inter-American Observatory, NOAO, which is operated by AURA, Inc., under cooperative agreement with the NSF; kolsen@noao.edu, csmith@noao.edu.

<sup>4</sup>Department of Astronomy, University of Washington, Seattle WA 98195; hodge@astro.washington.edu.

<sup>5</sup>WIYN Observatory, P. O. 26732, Tucson, AZ 85726-6732; jacob@wiyn.org.

<sup>6</sup>Participant in the Research Experiences for Undergraduates (REU) program at Lowell Obs., summer 2006. Present address: Five College Astronomy Dept., Smith College, McConnell Hall, Northampton, MA 01063; rmcneill@email.smith.edu.

<sup>7</sup>Participant, REU program at CTIO, 2001. Present address: Department of Astronomy, RLM 16.318, University of Texas, Austin, TX 78712-1083; sholmes@astro.as.utexas.edu

in these objects given its large WR population. The bright stars of intermediate color in the CMD are badly contaminated by foreground stars (30-100%), and considerable spectroscopy is needed before statistics on the yellow supergiants in these systems will be known. This study is intended to serve both as the impetus and “finding charts” for further space-based imaging, and for many spectroscopic programs at large aperture.

*Subject headings:* catalogs — galaxies: stellar content — stars: early-type — supergiants — surveys

## 1. Introduction

Studies of the resolved stellar content of nearby galaxies provide the only direct way of determining the effect that metallicity and other environmental factors play in the formation and evolution of massive stars. For instance, determinations of the initial mass function (IMF) in SMC, LMC, and Galactic clusters have established that no statistically significant differences are seen in the slope of the IMF (Massey 1998a; Elmegreen 1999; Kroupa 2001; Massey 2003). Similarly, evolutionary models of massive stars do a good job of matching the distribution of main-sequence stars in the H-R diagrams of the Magellanic Clouds (Massey et al. 1995b), and the location of red supergiants in the SMC, LMC, and Milky Way (Levesque et al. 2005, 2006). However, the range of metallicity in such studies is only a factor of four (SMC to Milky Way). With the advent of multi-object spectrographs on 8-m class telescopes it is now possible to push such studies to the more distant galaxies of the Local Group and beyond, where the range of metallicities is a factor of 20-30, and which include examples of both relatively quiescent galaxies and energetic starburst systems. (See Table 1 of Massey 2003, plus Table 1 of the present paper.)

This is the second of three papers presenting the results of our survey of the stellar content of Local Group galaxies currently forming stars. We used the 4-m telescopes at Kitt Peak and Cerro Tololo with the Mosaic CCD cameras to obtain images in *UBVRI*, as well as 50Å-wide interference filters centered on H $\alpha$ , [OIII], and [SII]. (Our survey excluded the SMC and LMC, which have been surveyed by other programs; see Massey 2002 and references therein, and Smith et al. 2005.) Our goal was to reach 2% photometry in the broad-band filters for massive stars, and to use the interference filter imaging to identify H $\alpha$  emission-lined stars. The first paper (Massey et al. 2006, hereafter Paper I) dealt with *UBVRI* photometry of stars in M31 and M33, the two spiral galaxies in our sample, and the third paper (McNeill et al. 2007) will discuss the identification and spectroscopy of the H $\alpha$  emission-lined stars in all nine of the galaxies in our sample.

We note that our primary goal is to lay out the photometry and CMDs as a first step for studying the massive stars of these systems. Many of these galaxies have had detailed studies (usually of small regions) with *HST* that have been used to constrain the star formation histories (SFHs) of these objects. While we provide cursory mention of some of these, the interested reader is referred to van den Bergh (2000) and others for a more complete discussion.

In this paper, we continue with an analysis of the broad-band photometry of seven dwarfs: IC10, NGC 6822, WLM, Sextans B, Sextans A, Pegasus, and Phoenix. We list their properties in Table 1. Of these, Sextans B and Sextans A are located in the outer fringes of the Local Group, and are probably not bound to the system (van den Bergh 1994), while the others are all true members and show varying degrees of current star formation (van den Bergh 2000). Regretfully, poor weather and limited observing time precluded the observation of IC1613, but we hope to rectify this omission in the future. Throughout this paper, we will discuss these galaxies in order of decreasing luminosity. In § 2 we describe our observations and reduction procedures, and present the photometry catalogs. In § 3 we will compare the color-magnitude diagrams (CMDs) in turn, and derive improved values of the reddenings of the complete sample (including M31 and M33). In § 4 we will summarize our results.

## 2. Observations and Data Reductions

The observation and reduction procedures for the Mosaic imaging data were described in considerable detail in Paper I, and we do not repeat these here, other than to note that the data were taken using dithered exposures and that the photometry was performed chip-by-chip on each individual exposure rather than on the combined image. Three southern galaxies (WLM, NGC 6822, and Phoenix) were observed with the CTIO Blanco 4-m telescope; the other four (IC10, Sextans B, Sextans A, and Pegasus) were observed at Kitt Peak with the Mayall 4-m. The two Mosaic cameras are nearly identical instruments, and consist of a two by four array of 2048x4096 SITe CCDs, yielding images contain 8192x8192 pixels. The scale of the final rectified images is  $0.27'' \text{ pixel}^{-1}$ . The field of view (FOV) of the Mosaic camera is  $35' \times 35'$ , but for three of the smaller galaxies (IC10, Sextans B, and Sextans A) observed at Kitt Peak we centered the galaxy on just one of the eight chips in order to avoid the effects of the ghost image caused by the Mayall’s prime focus corrector. A fourth galaxy observed at Kitt Peak, Pegasus, was centered on the array, but the calibration data extends only over the central 4 chips, as described below.) The journal of observations is given in Table 2, where we have included the average delivered image quality (DIQ) on our frames.

One of the strengths of our survey has been the large field of view ( $35' \times 35'$ ) in a single field. The spirals described in Paper I required multiple fields (M31, ten fields; M33, three fields) for good areal coverage. For the galaxies studied here, a single field was sufficient, and even so, the large FOV might seem wasted, given the small angular extent of some of these galaxies. However, the large areal coverage proved useful for determining the contribution made by foreground Galactic stars to the color-magnitude diagrams (CMDs). In Figs. 1 through 7 we show the fields of view corresponding to the calibrated photometry for each of the seven dwarfs. For IC10 and NGC 6822 this provides both complete coverage and a good sampling of the Milky Way foreground; in the case of the smaller systems (such as Sextans B) the galaxies are almost lost in the field. Of course, another strength is that the sampling is quite good ( $0.27'' \text{ pixel}^{-1}$ ), and to demonstrate this we have included enlargements of interesting areas<sup>1</sup>.

However, the primary strength of our survey is, we believe, in the high accuracy of our photometric calibration. Since each CCD has slightly different color responses, we decided to treat each of the eight CCDs in each camera as a separate instrument. The 150s readout time made it impractical to observe the large number of standard stars required to determine satisfactory transformation equations for each chip: simply observing one set of standards on each chip in all five filters would require  $\sim 1.5$  hrs just in reading out the array. Instead, we chose the philosophy of providing an external calibration for each field using time on smaller telescopes. That allowed us to devote most of each calibration night to observing standard stars, which were carefully chosen from the best-calibrated stars in Landolt (1992). This allowed extinction and color terms to be determined to high accuracy, and allowed us to determine highly accurate secondary calibration for each galaxy field. We found in Paper I that the method worked well, as judged by the milli-magnitude agreement for the results found for stars in overlapping fields in the M31 and M33 data. Furthermore, that study demonstrated that we were right to be concerned about the differences in the color-terms from chip to chip, as these would have introduced unacceptably large errors in the derived colors of stars had we simply used a single color term for each filter. Of course, the calibration images need to include some of the area for all the chips of interest. This decision also allowed us to make use of mostly clear but not-quite photometric nights for the 4-m Mosaic imaging, vastly reducing the amount of 4-m time needed for the project. That said, a little time was spent on the second CTIO Mosaic night observing a few Landolt fields;

---

<sup>1</sup>The imaging data are available through the NOAO Science Archive at <http://archive.noao.edu/nsa/>, as well as the Lowell ftp site <ftp://ftp.lowell.edu/pub/massey/lgsurvey/datarelease/>. In addition, we have made full resolution versions of Figs 1 through 7 available from our web site, <http://www.lowell.edu/users/massey/lgsurvey>.

these observations served primarily as a “reality check” on the derived color terms, as shown below.

For the galaxies with Mosaic data from the CTIO 4-m (WLM, NGC 6822, and Phoenix), we used the CTIO 0.9-m telescope and Tektronix 2048x2048 CCD to obtain *UBVRI* images of four 13.5'x13.5' fields for each galaxy. The fields were each offset from the galaxy coordinates by  $\pm 17.5'$  north-south and east-west in order to provide some overlap with all 8 chips in the Mosaic fields. These calibration data were all taken on the night of 2001 September 17 (UT). For the galaxies with Mosaic data from the Kitt Peak 4-m, we used the Lowell Observatory 1.1-m Hall telescope and SITe 2048x2048 CCD (FOV 19.4'x19.4') to obtain *UBVRI* images of the galaxy field. For M31 and M33 (Paper I) we had used two pointings, offset by 500" north and 500" south of each galaxy field, so as to provide overlap with the regions covered by all 8 Mosaic chips, but since most of the dwarfs are small, we simply obtained a single 20'x20' field centered on the galaxy for Pegasus, Sextans B, and Sextans A. We also included NGC 6822 (using the two pointings) and WLM (using a single pointing) in order to provide overlap in the calibration between the northern galaxies and the southern. The Lowell data were obtained on 2001 September 26 (IC10), 2001 October 14 (WLM and Pegasus), 2002 September 10 (NGC 6822), and 2002 November 2 (Sextans A and Sextans B).

For the northern hemisphere Mosaic data we adopted the color terms from Paper I. These were based upon averages of 13 independent calibrations (10 fields in M31 and 3 in M33). For the southern hemisphere Mosaic data, we used both the CTIO 0.9-m and Lowell 1.1-m calibrations of NGC 6822 to determine the color terms for all 8 chips. We give these values in Table 3. Although these are not as well determined as the Kitt Peak coefficients (as they are based upon fewer data), the agreement was very good between the Lowell and CTIO calibration data for NGC 6822 and WLM, with the exception of the  $R - I$  color term. For those, we used observations with standards observed with the Mosaic camera itself to determine that the CTIO 0.9-m calibration was better, and we adopted those values. Once the CTIO color-terms were fixed to the values in Table 3, we then determined the photometric zero-point in a chip-by-chip manner for each dithered Mosaic exposure for WLM, NGC 6822, and the Phoenix dwarf using the combined Lowell and CTIO catalogs for WLM and NGC 6822, and the CTIO catalog for the Phoenix dwarf.

We can test how well this procedure worked by comparing the agreements between the final catalogs of WLM and NGC 6822 stars and the individual Lowell 1.1-m and CTIO 0.9-m calibrating catalogs for these galaxies. We show the median differences in Table 4, where we have restricted the sample to stars with small photometric errors ( $< 0.01$  mag) and which were uncrowded. We consider the agreement quite good, although it is not of the same accuracy as that of the M31 and M33 data in Paper I, simply owing to the far sparser fields

for the dwarfs.

We present the final photometry catalogs in Tables 5 through 11 for the seven dwarfs. As with Paper I, we have chosen to make the catalogs coordinates based, with the designation LGGs J001956.99+591707.5 referring to the IC10 star whose coordinates are  $\alpha_{2000} = 00^h19^m56.99^s$  and  $\delta_{2000} = +59^\circ17'07.5''$ . Shortly after Paper I was published we discovered a minor problem in this M31 and M33 catalogs: in regions of extreme crowding there are sometimes two stars within  $0.1''$  of each other, and thus two stars might have the same designation. There were 62 cases of this in M31 (out of 371,781 stars), and 23 cases in M33 (out of 146,622 stars). There were no cases where 3 or more stars were involved. We have avoided this problem here by using an “A” for the brightest star, and a “B” for the fainter star. Since the photometry of stars this crowded is quite dubious, these designations serve primarily as flags that multiple components were identified. Rather than allow this confusion to persist in the M31 and M33 catalogs, we are making revised versions available here in on-line form, as Tables 12 and 13.

In Table 14 we show the typical (internal) errors of this photometry. Consistent with the exposure times and conditions given in Table 2, we found that the errors as a function of magnitude were comparable for Phoenix, Sex B, Sex A, and Pegasus. The galaxies NGC 6822 and WLM had somewhat smaller errors at a given magnitude. Given our efforts to compensate for the large reddening in IC10, the errors for that galaxy are smaller still. We also show the spread in errors in Fig. 8.

Our stated goal was to achieve 1-2% photometry for massive ( $> 20M_\odot$ ) stars. Did we achieve this? In Table 15 we list the expected brightness of a  $20M_\odot$  star in *UBVRI*, where we have adopted the distances and reddenings from Table 1, and intrinsic colors following Bessell et al. (1998) and FitzGerald (1970). We adopt the reddening excesses given by Schlegel et al. (1998), using their values for the “CTIO *UBVRI* system”, as the filter responses and CCD quantum efficiency is similar to ours. (We include values for M31, M33, the LMC, and SMC to aid in interpreting the CMDs later.)

First, let us consider the most heavily reddened galaxy in our sample, IC10. A  $20M_\odot$  star on the zero-age main sequence (ZAMS) will be quite faint at *U* (23.2), with correspondingly large errors (12%). Still, our efforts to compensate for the reddening by going quite deep at *B*, *V*, and *R* in IC10 were largely successful, and although we did not achieve 1-2% photometry, we did do better than 5% for such a star. At an age of 8 Myr, when the star is at the end of its main-sequence life (i.e., on the terminal age main sequence, TAMS), and the star is an early B-type supergiant, the photometric errors would be quite small, even at *U*. During its He-burning red supergiant (RSG) phase, the star would be invisible at *U*, but have small photometric errors ( $< 1\%$ ) in the other bandpasses, even *B*.

For a  $20M_{\odot}$  star in the other galaxies a comparison of Tables 14 and 15 show that we achieved our goals, except for the  $U$ -band during the RSG phase. Since we require that a star be detected in  $B$ ,  $V$ , and  $R$  to be included in the catalog, but not  $U$  or  $I$ , this should not have any effect on whether or not a RSG is included in our catalogs.

We provide a graphical representation of what we achieved in Fig. 9. The large colored dots show the absolute magnitude in each bandpass (i.e.,  $M_U$ ,  $M_B$ , etc.) for a  $20M_{\odot}$  star on the ZAMS (blue dots), on the TAMS (green dots), and as a RSG (red dots). For each galaxy, we use a colored line to show where we achieved 2% photometric errors in general. Thus we can see that we readily achieved 2% or better photometry for the TAMS, but that for IC10, Sextans A, and Sextans B we didn’t quite achieve this for the ZAMS. This underscores the point made by Rousseau et al. (1978) and re-emphasized by Massey et al. (1995b): massive stars evolve at essentially constant bolometric luminosity, but that means that a star near the ZAMS will be much fainter optically than when the star is “middle-aged” (half way between the ZAMS and the TAMS) simply owing to the fact that the high temperatures result in very large bolometric corrections. Our photometry came close to meeting our original goals, and the analysis presented here allow us to understand its actual limitations.

### 3. Results and Analysis: What the Color-Magnitude Diagrams Tell Us

Perhaps the clearest and most useful way to understand what our considerable photometry is telling us about these galaxies is by the most classical approach possible: comparing the color-magnitude diagrams (CMDs) of these systems. In Figs. 10 through 20 we present  $V$  vs  $B - V$  plots for all of the galaxies in our sample. To facilitate comparisons, we have also included M31 and M33 (from Paper I) and the LMC and SMC (from Massey 2002). In order to show the outstanding bright members, we have plotted the individual stars (rather than using Hess diagrams) but for illustrating the more densely populated regions of the CMDs we have included contours of equal star numbers. (We are indebted to Lynne Hillenbrand for suggesting this approach.) In general, we can distinguish four general regions of these diagrams: the blue supergiants on the left, the red supergiants (RSGs) on the right, and two sequences of (mainly) foreground stars near  $B - V \sim 0.6$  and  $B - V \sim 1.6$  for the galaxies at modest galactic latitudes. In order to minimize the effect these foreground stars have on the CMDs, we have restricted these diagrams to a subset of the field centered on the galaxy, as described in each figure caption. Of course, these last two regions will also contain a few bona-fide supergiants, but these are rare, and their identification will require a great deal of spectroscopy. The less luminous galaxies (those with  $M_V > -13$  in Table 1) have no discernible population of RSGs, owing to their scant number of massive stars.

### 3.1. Degree of Foreground Contamination

In interpreting the CMDs it is necessary to understand the degree of foreground contamination. For this reason, we have constructed CMDs of neighboring regions for each of the dwarf galaxy fields. We also use an updated version of the Bahcall & Soniera (1980) model of the Milky Way, kindly provided by Heather Morrison, to estimate the constituents of this contamination, and provide an estimate of the correction for our comparison data (M31, M33, the LMC, and the SMC).

By way of illustration, let us begin by considering the CMD of NGC 6822, which is located near to the plane of the Milky Way ( $b = -18.4^\circ$ ). In Fig. 15 (left) we see three sequences of bright stars ( $V < 20$ ), which we have labeled “blue supergiants”, “foreground and yellow supergiants”, and “red supergiants”, in describe their major constituents. In Fig. 15 (middle) we show the CMDs of the neighboring foregrounds fields. In the foreground field (which covers the same area) there are two primary sequences: one of intermediate color, which (by eye) seems to contain the same number of stars as in the NGC 6822 CMD, merging into a sequence of redder, fainter stars.

What fraction of the stars in this region of intermediate color are expected to be foreground, and which will be yellow supergiants? By eye it would appear that foreground objects will dominate overwhelmingly. Consider only the stars with  $16 < V < 20$  and  $0.5 < B - V < 1.4$ . We count 1052 stars in this region of the CMD for NGC 6822, which includes an area of  $0.052 \text{ deg}^2$ . We count stars in neighboring regions (whose areas sum to that used for NGC 6822), and find 991 stars, suggesting that the degree of contamination is about 94%. (Recall that we would expect variations of  $\sqrt{N}$  in either group, so really this should be viewed as  $94 \pm 4\%$ .) The Bahcall & Soneira (1980) model predicts a similar but somewhat smaller number of stars (852) in this region of the CMD. Of these, the model shows that 68% are disk dwarfs, 12% are halo dwarfs, and 20% are halo giants.

Next, let us consider the other extreme, the CMD of WLM, which is located far from the plane of the Milky Way, at a Galactic latitude  $b = -73.6^\circ$ . In the CMD (Fig. 16(left)) we find only a few bright  $16 < V < 20$  stars with intermediate colors ( $0.4 < B - V < 1.0$ ), where again we have restricted the CMD to only those stars near the galaxy, a region of  $0.023 \text{ deg}^2$ . We count only 20 stars in this region of the CMD. In the foreground field (Fig. 16 (middle) we count 19 stars within this region of the CMD, suggesting 95% contamination by foreground objects. The Bahcall & Soniera (1980) model again slightly underestimates the degree of contamination, predicting only 13 stars, of which only 10% will be disk dwarfs, while 55% will be halo dwarfs and 34% will be halo giants. So, even in this galaxy the



foreground contamination dominates for bright stars at intermediate colors<sup>2</sup>.

It is of course coincidental that in both cases we find a contamination of  $\sim 95\%$ : for NGC 6822 the low galactic latitude leads to a very substantial foreground component, but the galaxy is also quite rich in stars. There are far fewer foreground stars in the field of WLM, but the galaxy is also considerably less rich.

For our comparison CMDs of M31, M33, the SMC, and the LMC, we do not have neighboring foreground fields to use with any of these four galaxies, but instead rely upon the Bahcall & Soniera (1980) models scaled to the appropriate areas. For each galaxy, foreground contamination is quite significant for intermediate colors. For M31 (Fig. 10) roughly 50% of the bright ( $15 < V < 20$ ) stars of intermediate color ( $0.4 < B - V < 1.1$ ) are expected to be foreground. According to the model, 86% will be disk dwarfs, 7% will be halo dwarfs, and 7% halo giants. For the redder ( $1.2 < B - V < 1.8$ ) bright stars ( $16 < V < 20$ ) we expect about 85% to be foreground, all of which should be disk dwarfs<sup>3</sup>. For M33, about 40% of the bright ( $15 < V < 20$ ) stars of intermediate color ( $0.4 < B - V < 1.1$ ) will be foreground stars, of which 73% will be disk dwarfs, 15% halo dwarfs, and 12% halo giants. For the redder ( $1.2 < B - V < 1.8$ ) bright stars ( $16 < V < 20$ ) we expect about 70% to be foreground, made up nearly exclusively of disk dwarfs.

For the LMC and SMC we consider brighter stars ( $11 < V < 15$ ) but find similar percentages. For the LMC CMD stars of intermediate color ( $0.4 < B - V < 1.1$ ), about 85% will be disk dwarfs, 9% will be disk giants, and 6% will be halo giants. For the SMC CMD bright stars of intermediate color ( $0.4 < B - V < 1.1$ ) about 45% will be foreground stars, of which 82% will be disk dwarfs, 6% disk giants, and 12% halo giants.

In our tests, we did find that the Bahcall & Soniera (1980) model usually underestimated the number of stars. For red stars, this can be by as much as a factor of two. For instance, for WLM we see from Fig. 16 (middle) that there is also significant contamination in the region of the CMD occupied by RSGs. We count 27 stars in the WLM field with  $16 < V < 20$  and  $1.1 < B - V < 1.9$ . The Bahcall & Soniera (1980) model predicts only 8.5 stars (32% contamination, all of them disk dwarfs) while in our actual background fields we count 20 (74% contamination).

---

<sup>2</sup>Bresolin et al. (2006) estimate the degree of foreground contamination in this region to be negligible. We are unable to reproduce their result.

<sup>3</sup>Note that the various foreground contributions were mislabeled in the CMDs of Paper I as “foreground dwarfs” and “foreground giants” for the intermediate and red colors, respectively. The same is true for the CMDs in Massey (2002).

It is true, however, that in recent years there is an increased appreciation of the large angular extent of these galaxies, due to (for instances) tidal tails. The best known of these is the extended tail of M31 (Ibata et al. 2001). It may be that even our Mosaic fields do not extend sufficiently far away to provide a clean foreground sample for the fainter stars. For instance, Komiyama et al. (2003) have identified NGC 6822 stars that have formed far ( $25'$ ) from the main body of the galaxy, tracing the H I distribution. A few of these stars may be visible as the clump of blue stars at  $V \sim 22$  visible in the CMD of our “foreground” field in Fig. 15(middle). Nevertheless, our foreground fields are useful for distinguishing the bona-fide massive star populations.

We summarize the degree of foreground contamination in Table 16, where we have chosen the regions of the CMD to examine by eye, and used the Bahcall & Soniera (1980) model to estimate the fractional contribution by different components of the Milky Way. Since the model occasionally underestimates the degree of contamination, these percentages are primarily illustrative.

### 3.2. Reddenings

We can use these CMDs to redetermine the reddening of these galaxies, by using the location of the plume of blue supergiants, following Massey & Armandroff (1995). We use as our references the CMDs of the LMC and SMC (Figs. 12 and 13), and adopt  $E(B-V) = 0.13$  and  $E(B-V) = 0.09$  for the two galaxies, respectively, following Massey et al. (1995a)<sup>4</sup>. We give the results of this analysis in Table 17.

The values in Table 17 apply to the typical OB star in each of these galaxies, although clearly there are regions that are more heavily reddened, particularly in M31. For comparison, we note that Massey et al. (1986) found reddenings for several OB associations in M31; i.e.,  $E(B-V) = 0.12$  for OB78 (NGC 206),  $E(B-V)=0.24$  for OB 48 and the OB 8-10

---

<sup>4</sup>Van den Bergh (2000) suggests that the Massey et al. (1995b) result of  $E(B-V) = 0.13$  for the LMC is possibly too low, noting that Harris et al. (1997) derive  $E(B-V) = 0.20$  from a larger sample. Massey et al. (1995b) used a sample of 414 LMC OB stars with known spectral types to derive a median reddening, comparing the observed  $B-V$  color with the intrinsic color expected for each spectral type. By contrast, Harris et al. (1997) used two-color diagrams to estimate the reddenings for 2069 (presumed OB) stars, and report a mean value. While there are certainly stars with higher reddenings in the Clouds, we retain the median values given by Massey et al. (1995b), as the method should be more accurate, despite the smaller sample size. We note that the agreement between the results of comparing the blue plumes of the various galaxies in our sample to that of the LMC and SMC give consistent results (at the  $\pm 0.02$  mag level) if we adopt the Massey et al. (1995b) values.

region, and  $E(B - V) = 0.08$  for OB 102. These values are consistent with our finding here that the typical reddening is  $E(B - V) = 0.13$ . Similarly, Massey et al. (1995a) used spectroscopic samples in NGC 6822 and M33 to determine reddenings of  $E(B - V) = 0.39$  and  $E(B - V) = 0.13$ , respectively. The value for NGC 6822 determined here is considerably lower (0.25), and we suggest that the few OB associations studied by Massey et al. (1995a) were higher in reddening than typical. This interpretation is consistent with the study by Bianchi et al. (2001) which finds  $E(B - V)$  varying from 0.25 to 0.45. Our value for M33's reddening is in very good agreement with that of Massey et al. (1995a). For IC10 Massey & Armandroff (1995) estimated  $E(B - V) = 0.75 - 0.80$  using their photometry of the blue plume; ours goes considerably deeper, allowing a more accurate determination, but one that is in good accord with this earlier finding.

How much of this reddening is attributable to foreground, and how much is internal to these galaxies themselves? We have used the  $100\mu\text{m}$  dust maps of Schlegel et al. (1998) to estimate the foreground  $E(B - V)$ , and we list these values in Table 17. (The low Galactic latitude of IC10 prevents an accurate determination.) The difference between these values and the total reddenings should give a good indication of how much is internal to these galaxies. We see that the median value is 0.05 mag, in good accord with what is commonly assumed for irregular galaxies (see Hunter & Elmegreen 2006).

We were initially skeptical of the relatively high reddenings found in Pegasus and Phoenix, the two lowest luminosity galaxies in our sample. However, Gallagher et al. (1998) found an identical value for the total  $E(B - V)$  in their two-color *HST* study of Pegasus. These galaxies are currently quite quiescent in forming stars (see Table 1) but dust is primarily contributed to the ISM via low-mass asymptotic giant branch (AGB) stars (see Whittet 2003). Both galaxies do show modest amounts of H I (Young et al. 2003, St-Germain et al. 1999).

### 3.3. The Massive Star Populations in Individual Galaxies

Using the results of the previous two sections, we have constructed CMDs which have been converted to absolute magnitude (using the distances and reddenings in Tables 1 and 17). These are included at the right of In Figs. 10 through 20. We have also cleaned out the foreground contribution, at least in a statistical sense, by using the foreground fields for seven dwarfs. For each star in the foreground CMD (middle panel of Figs. 14 through 20) we have removed a star near that position in the galaxy CMD. The process is only approximate; if no star was within 0.2 mag in  $B - V$  and 0.8 mag in  $V$  of a foreground star, we did not use it. For the CMDs of galaxies lacking foreground fields (Figs. 10-13), we use the Bahcall

& Soneria (1980) models to predict the number of foreground stars in each 0.1 mag  $B - V$  bin and each 1 mag  $V$  bin. Of course, this is considerably cruder and less certain, and many objects which are doubtless foreground are left, but the resulting CMDs are still quite illustrative.

### 3.3.1. IC10

IC10 is the most luminous galaxy in our sample of dwarfs (see Table 1), and it is also the most heavily reddened due to its low Galactic latitude. Massey & Armandroff (1995) argued that the galaxy is in a starburst phase, based upon the current high star-formation rate, as judged by the known high  $H\alpha$  luminosity compared to either its H I mass or blue-light luminosity (Hunter & Gallagher 1986; Thronson et al. 1990; Hunter et al. 1993), and in accord with its extremely large number of Wolf-Rayet (WR) stars detected at the time (Massey et al. 1992). Massey & Armandroff (1995) found that surface density of WR stars, averaged over *the entire galaxy*, is roughly comparable to the most WR-rich OB associations in M33. Since that time additional WRs have been found (Massey & Holmes 2002, Crowther et al. 2003), and as discussed by Massey & Holmes (2002), a new survey suggests that the actual number of WRs in IC10 may be considerably higher than previously thought.

In Table 18 we give the cross-references between our photometry catalog and the stars with known spectral types from the literature. In the case of IC10 these are all from spectroscopy of WR candidates. The identifications have been checked by eye against the finding charts published by Crowther et al. (2003); this was necessitated by crowding and the ambiguity of the “system” on which some of the published coordinates were based (i.e., Guide Star Catalog vs USNO-B). However, in some cases we found that stars previously identified as single were in fact identified as multiple on our PSF-fitting; i.e., [MAC 92] 2, RSV9, and [MAC 92] 7. Others were recognized as multiple by Crowther et al. (2003); e.g., [MAC 92] 17 and [MAC92] 24. For these cases the blending is sufficiently bad, and the photometric difference between components sufficiently slight, that we cannot reliably determine which component is the WR star. Following Crowther et al. (2003) we examined the *HST* images of these stars using in particular the newer ACS data available since the time of the Crowther et al. (2003) study. While these images in general confirmed our identification of multiple sources, they did not shed any useful light on which component was the WR star. Therefore we list the multiple components in Table 18 where appropriate. We have adopted the revised spectral types of the WRs given by Crowther et al. (2003) based upon their new spectroscopy of WRs previously confirmed spectroscopically (Massey et al. 1992; Massey & Armandroff 1995; Massey & Holmes 2003), plus a few of their own candidates,

although it was not always clear if their data were of higher quality or if they were simply bolder in assigning exact spectral subtypes (i.e., “WC4” vs “WC”). The exceptions are the instances where they chose to reclassify a star based solely upon their interpretation of the illustrations of spectra published by others. Only the WR star RSMV 13 was too faint to be included in our catalog.

In Fig. 14 (left) we show the unfiltered CMD for IC10. In comparing this to that of the unfiltered SMC CMD, we are struck first by the large amount of reddening. The foreground sequence is very tilted, as expected very close to the plane of the Milky Way, as more distant stars will be more heavily reddened, and the line of sight goes through a substantial part of the Galaxy. (In the other galaxies, the foreground CMDs are nearly vertical, as one quickly runs past the edge of the dust plane.) The blue supergiants have been shifted from their peak near 0 in the SMC and LMC to roughly 0.7 in IC10. In Fig. 14 (right) we see the dereddened CMD converted to absolute magnitude with the foreground contamination largely removed.

The second most noticeable fact about the CMD of IC10 given in Fig. 14 is the relative dearth of RSGs. Massey (2002) found that the relative number of WRs and RSGs was extremely well correlated with metallicity in the Local Group, at least for the SMC, NGC 6822, the LMC, M33, and M31. The metallicity of IC10 is intermediate to that of the SMC and LMC, and has an intermediate number of WR stars (26 confirmed, to the SMC’s 12 and the LMC’s 130; see Crowther et al. 2003, Massey & Holmes 2002, Massey 2003, and Massey & Duffy 2002.) So, one should expect a RSG branch that is similar in absolute numbers intermediate to the SMC and LMC, and a comparison of Figs. 14 with 13 and 12 shows that we are clearly *not* seeing that. (Massey & Holmes 2003 estimate that the true number of WRs in IC10 is about 90, which should imply even more RSGs.) Where, then, are the missing RSGs?

We don’t know how long the burst of star-formation has been going on in IC10, only that the amount of gas cannot sustain the present amount of star formation for a significant fraction of a Hubble time (see discussion in Massey & Armandroff 1995). The typical age of a star in the WR phase is 3-4 Myr, while the ages of RSGs will be 10-20 Myr. Thus, if IC10’s burst is extremely young, say 10 Myr, that would explain the lack of RSGs while allowing the large population of WRs. As we note in discussing NGC 6822, this lack of RSGs is consistent with the luminosities of the visually brightest blue supergiants.

### 3.3.2. NGC 6822

The first comprehensive study of the resolved stellar population of NGC 6822 was that of Kayser (1966, 1967), whose photographic photometry identified blue supergiants, and a sequence of RSGs. Some of the latter were shown to be variable. It is instructive to compare her CMD (Kayser 1967 Fig 3) to ours (Fig. 15 left). Although ours goes deeper, of course, the general characteristics are similar. In our figure we find that the blue supergiants are well distinguished from the foreground dwarfs, despite the large number of the latter, due to NGC 6822’s relatively low Galactic latitude ( $b = -18.4^\circ$ ). In its CMD we see a strong RSG component starting at  $B - V = 1.8$  and  $V = 19.5$  and extending to  $B - V > 2$  and possibly  $V = 17.5$ , much as Kayser (1966, 1967) found. Massey (1998b) obtained spectra of several of these RSGs.

By contrast to IC10, NGC 6822 contains only 4 WRs, and it is likely this number is complete (Massey & Johnson 1998). A comparison of the CMDs of NGC 6822 (Fig. 15 left) and IC10 (Fig. 14 left) is quite instructive: we expect stars to be shifted about 1.7 mag fainter in IC10 and to 0.55 redder colors. The tip of the “blue plume” in NGC 6822 is at about  $V = 18$ , and we see that in IC10 this is more like  $V = 21$ —although IC10 does have a large number of WRs, the (visually) brightest blue supergiants are not visible in similar numbers. Recall, though, that the brightest blue supergiants in  $V$  are the evolved A-type supergiants from intermediate high mass stars ( $10\text{--}25M_\odot$ ) with an age similar to RSGs; thus this comparison shows consistency between the strong blue and red supergiant populations of NGC 6822, and the relatively weak population of *visually* bright blue supergiants and lack of RSGs in IC10.

Only 38 of NGC 6822’s massive stars have been observed spectroscopically, and we list those in Table 19<sup>5</sup>. The WRs are identified by the designations given in Massey & Johnson (1998), while the OB stars are primarily identified by the OB association designations given in Massey et al. (1995a). Red supergiants were identified from spectroscopic photometry by Massey (1998b); in some cases these lack spectral types, but the strengths of the CaII triplet and radial velocities have been used to show these are members. In addition, there are a few early- and late-type supergiants that were observed spectroscopically by Humphreys (1980a). These are referred to only by the designations given in the photographic reproductions in the PhD thesis of Kayser (1966), with no coordinates provided. The reproduction of these plates are usually not readable in the copies of this thesis that are available commercially. However,

---

<sup>5</sup>Bianchi et al. (2001) and Catanzaro et al. (2003) observed several additional stars in the NGC 6822, but no spectral types are given, apparently due to the poor signal-to-noise of their spectra.

an excellent copy is now available electronically<sup>6</sup>, and we used this to cross reference the stars with spectroscopy by Humphreys (1980a) to our survey.

NGC 6822 is one of the few galaxies in our sample for which previous ground-based photometry has been published covering most of the galaxy. We provide a comparison to the work of Bianchi et al. (2001) in Fig. 21. Out of the 3232 stars in Bianchi et al. (2001)’s catalog, we found 3135 matches to our Mosaic catalog, where we have restricted the latter sample to only those stars with errors less than 0.1 mag. We had to adjust the Bianchi et al. (2001) coordinates by  $-0.05''$  and  $-0.17''$ , due to the need to transform from the Guide Star Catalog system used by Bianchi et al. (2001) to that of USNO-B, which we use here. The photometry agrees extremely well in that the median differences are 0.03 mag in  $V$ , 0.002 mag in  $B - V$ , and 0.020 mag in  $U - B$ , all in the sense of our values minus those of Bianchi et al. (2001). However, it is clear from Fig. 21b that there is a significant color term in  $B - V$ : the bluest stars in our catalog appear slightly less blue in Bianchi et al. (2001), while the red stars in our sample are redder than in Bianchi et al. (2001). No independent  $UBV$  calibration was obtained for the ground-based data of Bianchi et al. (2001), but rather their photometry was tied to the Massey et al. (1995) study of OB stars in several small regions in NGC 6822, which covered a more modest color range than here<sup>7</sup>. For  $U - B$  (Fig. 21c) there is a modest color term for the reddest stars, and in addition there is a sequence of stars that are much redder in the  $U - B$  of Bianchi et al. (2001) than in the present study. The size of the color term is not unexpected, as Bianchi et al. (2001) warn that the reddest stars might be systematically affected by errors at the 0.1 mag level. The sequence of much redder stars is harder to understand. To investigate this further, we selected only the stars with differences  $> 0.5$  mag in  $U - B$  and show these stars plotted against  $B - V$  in Fig. 21d. It is clear that the problem occurs primarily around a  $B - V$  of 0, where stars in Bianchi et al. (2001) may show *much* redder  $U - B$  values than their  $B - V$  warrants. Massey (2002) has reported similar problems in  $U - B$  CCD photometry near  $B - V \sim 0$ , owing to the usual mismatches of the intrinsic filter plus detector bandpass compared to the standard bandpass, and the size of the Balmer jump.

---

<sup>6</sup>See <http://etd.caltech.edu/etd/available/etd-09232002-112325>. We are indebted to Cathy Slesnick for tracking this down.

<sup>7</sup> The first author of the present paper was responsible for the reduction of the ground-based photometry of Bianchi et al. (2001).

### 3.3.3. WLM

It is clear from Fig. 16 that WLM is still relatively rich in massive stars, at least compared to the lower luminosity galaxies (Figs. 17-20), as shown by the strength of the “plume” of blue stars with  $B - V \leq 0.2$ . The galaxy is far from the Galactic plane ( $b = -73.6^\circ$ ), and has minimal reddening (Minniti & Zijlstra 1997, and our Table 17). Nevertheless, as discussed in § 3.1, the vast majority of bright ( $16 < V < 20$ ) stars of intermediate color ( $0.4 < B - V < 1.1$ ) are foreground.

Five WLM stars were confirmed spectroscopically as early-type supergiants by Venn et al. (2003), and these plus an additional 33 stars were observed spectroscopically by Bresolin et al. (2006). The fact that all 38 of these stars could be observed in just a little over two hours of integration with the VLT emphasizes the power of modern large telescope with multi-object spectroscopic capabilities; this number is the same as the number of stars observed spectroscopically over the past 27 years in the considerably better studied galaxy NGC 6822 (Table 19). Bresolin et al. (2006) identified primarily B and early A supergiants, as well as two O stars. They also identified four G-type supergiants. The fact that all four of these stars of intermediate color were supergiants is rather surprising, as these stars are found in a region of the CMD where we expect a significant foreground contribution (Fig. 16 (middle)). Using the Bahcall & Soniera (1980) model we compute that for  $18 < V < 21$  and  $1.0 < B - V < 1.8$  (the range covered by their G supergiants) we expect 35 foreground stars; in good agreement with the 43 stars we count from our neighboring foreground fields. There are 84 stars in this part of the CMD, so we would expect about 40-50% to be foreground. (In contrast, Bresolin et al. 2006 suggest that the foreground contribution is negligible, a conclusion with which we do not agree.) The luminosity criteria used by Bresolin et al. (2006) is based on an empirical relation between the equivalent width of  $H\gamma$  and the luminosity class found for somewhat earlier type (O9-F8) stars, as their dispersion was relatively low ( $5\text{\AA}$ ). Further work may be needed to clarify the exact nature of these four stars, as halo giants would have radial velocities similar to that of the WLM.

Several groups have obtained and discussed global, ground-based photometry of this galaxy (Minniti & Zijlstra 1997, McConnachie et al. 2005) but not published the individual values. Bresolin et al. (2006) list  $V$  and  $V - I$  photometry of their 38 spectroscopic candidates, based upon some as yet unpublished photometric study. Excluding the one blended object (J000158.73-153001.5) and one outlier in color (J000156.62-152501.5) we find very good agreement in the photometry, with a median difference  $V(\text{Mosaic}) - V(\text{Bresolin}) = -0.03$  and  $V - I(\text{Mosaic}) - V - I(\text{Bresolin}) = -0.01$ . Deep *HST* photometry has been analyzed by Dolphin (2000) and Rejkuba et al. (2000).



### 3.4. The Other Galaxies

Spectroscopy has not yet been carried out for the stars in the other four galaxies, and so we just discuss them briefly here.

Although Sextans B is more luminous than Sextans A (Table 1) it is clear from comparing the CMDs (Figs. 17 and 18) that there are considerably more massive stars present in Sextans A. Both show some enhancement of bright red stars over the adjacent foreground fields, and so it is likely that these galaxies contain some RSGs.

Analysis of deep CCD photometry of Sextans B has been published by Sakai et al. (1997), but individual measurements were not published other than for a hand full of stars identified only on the finding charts of Sandage & Carlson (1985a), and we have not done the matching that would be needed to compare our results. (See also Piotto et al. 1994). Deep *HST* photometry of a part of Sextans A has been analyzed by Dohm-Palmer et al. (1997a,b).

Pegasus contains only a smattering of blue supergiants (compare the CMD of the galaxy field (Fig. 19 (left)) with that of the neighboring foreground field (Fig. 19 (middle))). These are apparent in Fig. 19 (right), in which we have subtracted the foreground, statistically. Even the lowest luminosity galaxy in our sample, Phoenix, contains a stronger blue supergiant population (Fig. 20). The primary difference is that Phoenix contains a very strong population of intermediate age stars, in accord with the findings of Canterna & Flower (1977). As such, Phoenix appears to be intermediate between an irregular galaxy and a dwarf spheroidal (van den Bergh 2000). Neither galaxy appears to have a significant number of RSGs.

Deep *BVR* photometry of Pegasus was discussed by Lee (1995a,b) but individual measurements were not apparently ever published. Lee (1995b) mentions the presence of bright RSGs in his CMD, but a comparison of our CMD of the galaxy (Fig. 19 (left)) with the CMD of neighboring foreground fields (Fig. 19 (middle)) makes this unlikely. Gallagher et al. (1998) have provided a very comprehensive study of the stellar populations of Phoenix based upon deep *HST* and ground-based imaging.

## 4. Summary and Future Work

We have obtained broad-band photometry of 88,144 stars (identified in *B*, *V*, and *R*) in IC10 (20,663 stars), NGC 6822 (51,877 stars), WLM (7,656 stars), Sextans B (800 stars), Sextans A (1,516 stars), Pegasus (1,390 stars), and Phoenix (4,242 stars). Combined with our

earlier work in Paper I on M31 (371,781 stars) and M33 (145,522 stars), our survey consists of over half a million stars with accurate coordinates and photometry. The corresponding images are available from our ftp site<sup>8</sup> or through NOAO<sup>9</sup>. Although our survey lacks the high angular resolution afforded by *HST*, it provides full areal coverage of these galaxies, including neighboring regions that can be used for evaluating the contribution of foreground stars to the CMDs; the photometry is also on a well-defined standard system that can be used for monitoring long-term variability. It is our hope that these data will serve both as the impetus and “finding charts” for further space-based imaging, and for many spectroscopic programs at large aperture.

We have inter-compared the CMDs of these systems and those of the Magellanic Clouds. This has led to improved estimates of the typical reddening of an OB star in these systems, based upon the colors of the plume of blue supergiants, and adopting the reddening values for the LMC and SMC based upon spectroscopy of hundreds of stars. The CMDs reveal strong or modest blue supergiants in all of these galaxies. All but Pegasus and Phoenix also show red supergiants in their CMDs, although we find a curious deficiency of RSGs in the starburst galaxy IC10. Without exception, the bright stars of intermediate color in the CMDs are strongly (30-100%) contaminated by foreground Galactic stars, a combination of disk and halo dwarfs, and halo giants.

Follow-up projects we plan in the near future include:

1. Determination of the IMF for massive stars at differing metallicities.
2. Identification of yellow supergiants (F-G I). Given the large foreground contamination, this will require spectroscopy of hundreds, and possibly thousands, of stars, but such studies can be readily accomplished by multi-object spectroscopy on 6.5-m class telescopes. Knowledge of the numbers of yellow supergiants would provide critical test of massive stellar evolutionary theories. Such stars would also provide a good astrometric reference, as they are relatively bright ( $V \sim 16$ ) and have negligible proper motion.
3. Spectroscopic confirmation of the RSGs in these systems, both to provide statistics on the relative number of red and blue massive stars at differing metallicities (for comparison with evolutionary models), and to provide targets for spectroscopic determinations of physical properties.
4. Determination of physical properties of blue supergiants at differing metallicities.

---

<sup>8</sup><ftp://ftp.lowell.edu/pub/massey/lgsurvey/datarelease/>

<sup>9</sup><http://archive.noao.edu/nsa/>

We are grateful for the encouragement of our colleagues in this project; help with the initial proposal was also provided by N. King and A. Saha. R.T.M. was supported through the NSF’s REU program, and we gratefully acknowledge AST-0453611.

## REFERENCES

- Bahcall, J. N., & Soneira, R. M. 1980, *ApJS*, 44, 73
- Bessell, M. S., Castelli, F., & Plez, B. 1998, *A&A*, 333, 231
- Bianchi, L., Lamers, H. J. G. L. M., Hutchings, J. B., Massey, P., Kudritzki, R., Herrero, A., & Lennon, D. J. 1994, *A&A*, 292, 213
- Bianchi, L., Scuderi, S., Massey, P., & Romaniello, M. 2001, *AJ*, 121, 2020
- Bothun, G. D. & Thompson, I. B. 1988, *AJ*, 96, 877
- Bresolin, F., Pietrzynski, G., Urbaneja, M. A., Gieren, W., Kudritzki, R.-P., & Venn, K. A. 2006, *ApJ*, in press, astro-ph/0605640
- Canterna, R., & Flower, P. J. 1977, *ApJ*, 212, L57
- Catanzaro, G., Bianchi, L., Scuderi, S., & Manchado, A. 2003, *A&A*, 403, 111
- Crowther, P. A., Drissen, L., Abbott, J. B., Royer, P., & Smartt, S. J. 2003, *A&A*, 404, 483
- Dohm-Palmer, R. C. et al. 1997a, *AJ*, 114, 2514
- Dohm-Palmer, R. C. et al. 1997b, *AJ*, 114, 2527
- Dolphin, A. E. 2000, *ApJ*, 531, 804
- Elmegreen, B. G. 1999, *ApJ*, 515, 323
- FitzGerald, M. P. 1970, *A&A*, 4, 234
- Gallagher, J. S., Tolstoy, W., Dohm-Palmer, R. C., Skillman, E. D., Cole, A. A., Hoessel, J. G., Saha, A., & Mateo, M. 1998, *AJ*, 115, 1869
- Harris, J., Zaritsky, D., & Thompson, I. 1997, *AJ*, 114, 1933
- Hubble, E., & Sandage, A. 1953, *ApJ*, 118, 353
- Humphreys, R. M. 1979, *ApJ*, 234, 854
- Humphreys, R. M. 1980a, *ApJ*, 238, 65
- Humphreys, R. M. 1980b, *ApJ*, 241, 587

- Humphreys, R. M., Massey, P., & Freedman, W. L. 1990, *AJ*, 99, 84
- Humphreys, R. M., Pennington, R. L., Jones, T. J., & Ghigo, F. D. 1988, *AJ*, 96, 1884
- Hunter, D. A., & Elmegreen, B. G. 2004, *AJ*, 128, 2170
- Hunter, D. A., & Elmegreen, B. G. 2006, *ApJS*, 162, 49
- Hunter, D. A., & Gallagher, J. S. 1986, *PASP*, 98, 5
- Hunter, D. A., Hawley, W. N., & Gallagher, J. S. 1993, *AJ*, 106, 1797
- Ibata, R., Irwin, M. J., Lewis, G. F., Ferguson, A. M. N., & Tanvir, N. R. 2001, *Nature*, 412, 49
- Kayser, S. E. 1966, PhD Thesis, California Institute of Technology
- Kayser, S. E. 1967, *AJ*, 72, 134
- Kennicutt, R. C., Edgar, B. K., & Hodge, P. W. 1989, *ApJ*, 337, 761
- Kennicutt, R. C., & Hodge, P. W. 1986, *ApJ*, 306, 130
- Komiyama, Y. et al. 2003, *ApJ*, 590, L17
- Kroupa, P. 2001, *MNRAS*, 322, 231
- Landolt, A. U. 1992, *AJ*, 104, 340
- Lee, M. G. 1995a, *J. Korean Astron. Soc.*, 28, 169
- Lee, M. G. 1995b, in *Stellar Populations*, IAU Symposium 164, ed. P. C. van der Kruit & G. Gilmore (Dordrecht: Kluwer), 413
- Levesque, E. M., Massey, P., Olsen, K. A. G., Plez, B., Josselin, E., Maeder, A., & Meynet, G. 2005, *ApJ*, 628, 973
- Levesque, E. M., Massey, P., Olsen, K. A. G., Plez, B., Meynet, G., & Maeder, A. 2006, *ApJ*, 645, 1102
- Massey, P. 1998a, in *ASP Conf. Ser. 142, The Stellar Initial Mass Function*, 38th Herstmonceux Conference, ed. G. Gilmore & D. Howell (San Francisco: ASP), 17
- Massey, P. 1998b, *ApJ*, 501, 153
- Massey, P. 2002, *ApJS*, 141, 81
- Massey, P. 2003, *ARA&A*, 41, 15
- Massey, P., & Armandroff, T. E. 1995, *AJ*, 109, 2470
- Massey, P., Armandroff, T. E., & Conti, P. S. 1986, *AJ*, 92, 1303
- Massey, P., Armandroff, T. E., & Conti, P. S. 1992, *AJ*, 103, 1159

- Massey, P., Armandroff, T. E., Pyke, R., Patel, K., & Wilson, C. D. 1995a, *AJ*, 110, 2715
- Massey, P., Bianchi, L., Hutchings, J. B., & Stecher, T. P. 1996, *ApJ*, 469, 629
- Massey, P., & Duffy, A. S. 2001, *ApJ*, 550, 713
- Massey, P., & Holmes, S. 2002, *ApJ*, 580, L35
- Massey, P., & Johnson, O. 1998, *ApJ*, 505, 793
- Massey, P., Lang, C. C., DeGioia-Eastwood, K., & Garmany, C. D. 1995b, *ApJ*, 438, 188
- Massey, P., Olsen, K. A. G., Hodge, P. W., Srong, S. B., Jacoby, G. H., Schlingman, W., & Smith, R. C. 2006, *AJ*, 131, 2478 (Paper I)
- McConnachie, A. W., Irwin, M. J., Ferguson, A. M. N., Ibata, R. A., Lewis, G. F., & Tanvir, N. 2005, *MNRAS*, 356, 979
- McNeill, R. T., Massey, P., Olsen, K. A. G., Hodge, P. W., Blaha, C., Jacoby, G. H., Smith, R. C., & Strong, S. B. 2007, in prep
- Minniti, D., & Zijlstra, A. A. 1997, *AJ*, 114, 147
- Monteverde, M. I., Herrero, A., Lennon, D. J., & Kudritzki, R. P. 1996, *A&A*, 312, 24
- Muschielok, B. et al. 1999, *A&A*, 352, L40
- Piotto, G., Capaccioli, M., & Pellegrini, C. 1994, *A&A*, 287, 371
- Rejkuba, M., Minniti, D., Gregg, M. D., Zijlstra, A. A., Alonso, M., V., Goudfrooij, P. 2000, *AJ*, 120, 801
- Rousseau, J., Martin, N., Prevot, L., Rebeiro, E., Robin, A., & Brunet, J. P. 1978, *A&AS*, 31, 243
- Sakai, S., Madore, B. F., & Freedman, W. L. 1997, *ApJ* 480, 589
- Sandage, A., & Carlson, G. 1985a, *AJ*, 90, 1019
- Sandage, A., & Carlson, G. 1985b, *AJ*, 90, 1464
- Schlegel, D. J., Finkbeiner, D. P., & Davis, M. 1998, *ApJ*, 500, 525
- Schommer, R., Smith, C., Olsen, K., & Walker, A. 2000, CTIO MOsaic II Imager User Manual, <http://www.ctio.noao.edu/mosaic/manual/index.html>
- Smith, R. C., Points, S. D., Chu, Y.-H., Winkler, P. F., Aguilera, C., Leiton, R., & MCELS Team 2005, in *BAAS* 207, 2507
- Sparke, L. S., & Gallagher, J. S. 2000, *Galaxies in the Universe: An Introduction* (Cambridge, Cambridge Univ. Press), 153
- St-Germain, J., Carignan, C., Cote, S., & Oosterloo, T. 1999, *AJ*, 118, 1235

- Thronson, H. A., Hunter, D. A., Casey, S., & Harper, D. A. 1990, *ApJ*, 355, 94
- Trundle, C., Dufton, P. L., Lennon, D. J., Smartt, S. J., & Urbaneja, M. A. 2002, *A&A* 395, 519
- Young, L. M., van Zee, L., Lo, K. Y., Dohm-Palmer, R. C., & Beierle, M. E. 2003, *ApJ*, 592, 111
- van den Bergh, S. 1994, *AJ* 107, 1328
- van den Bergh, S. 2000, *The Galaxies of the Local Group* (Cambridge: Cambridge Univ. Press)
- van den Bergh, S., Herbst, E., & Kowal, C. T. 1975, *ApJS*, 29, 303
- Venn, K. A. et al. 2001, *ApJ*, 547, 765
- Venn, K. A., Tolstoy, E., Kaufer, A., Skillman, E. D., Clarkson, S. M., Smartt, S. J., Lennon, D. J., & Kudritzki, R. P. 2003, *AJ*, 126, 1326
- Walterbos, R. A. M. & Kennicutt, R. C., Jr. 1988, *A&A*, 198, 61
- Whittet, D. C. B. 2003, *Dust in the Galactic Environment* (Bristol: IOP)
- Wilson, C. 1992 *AJ*, 104, 1374



Fig. 1.— IC10 Mosaic field. The region on the left shows the entire 20'x30' calibrated region. The region on the right shows an enlargement of a 6'x6' section near the center.



Fig. 2.— NGC 6822 Mosaic field. The region shown on the left is the entire 35'x35' FOV, all of which was calibrated. The region on the right shows an enlargement of a 6'x6' section in the NW corner of the galaxy.





Fig. 3.— WLM Mosaic field. The region shown on the left is the entire  $35'\times 35'$  FOV, all of which was calibrated. The region on the right shows an enlargement of a roughly  $3.7'\times 3.7'$  section south of the galaxy's center.



Fig. 4.— Sextans B Mosaic field. The region shown on the left is the 20'x30' calibrated region. The region on the right shows an enlargement of a roughly 3.8'x3.8' section near the middle of the galaxy.



Fig. 5.— Sextans A Mosaic field. The region shown on the left is the 20'x30' calibrated region. The region on the right shows an enlargement of a roughly 6'x6' section centered on the galaxy.

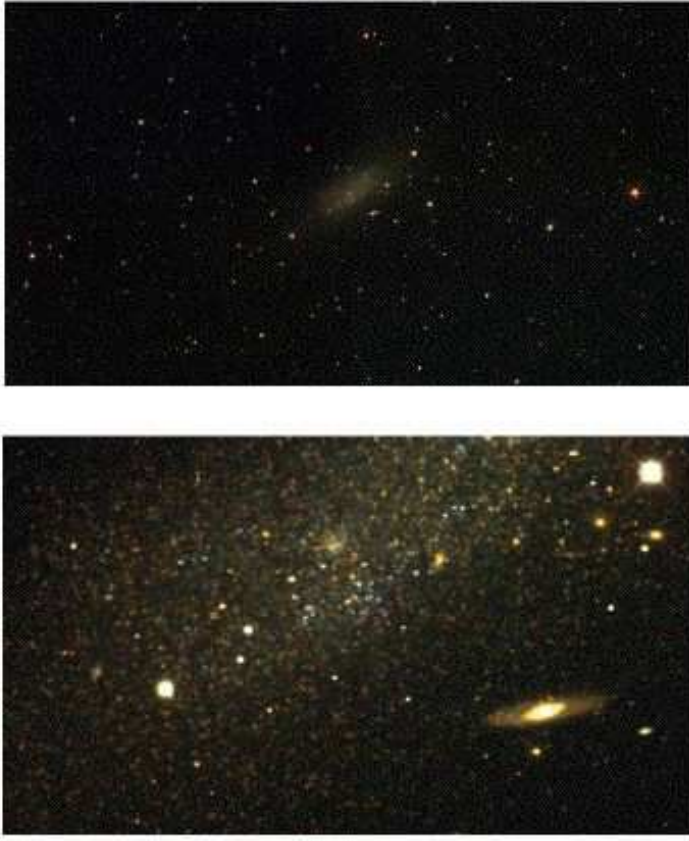


Fig. 6.— Pegasus Mosaic field. The region shown on the top is the 20'x30' calibrated region. The region below it an enlargement of a roughly 4.2'x2.4' section south of the center of the galaxy.



Fig. 7.— Phoenix Mosaic field. The region shown on the left is the entire 35'x35' FOV, all of which was calibrated. The region on the right shows an enlargement of a roughly 4.5'x4.5' section centered on the galaxy.

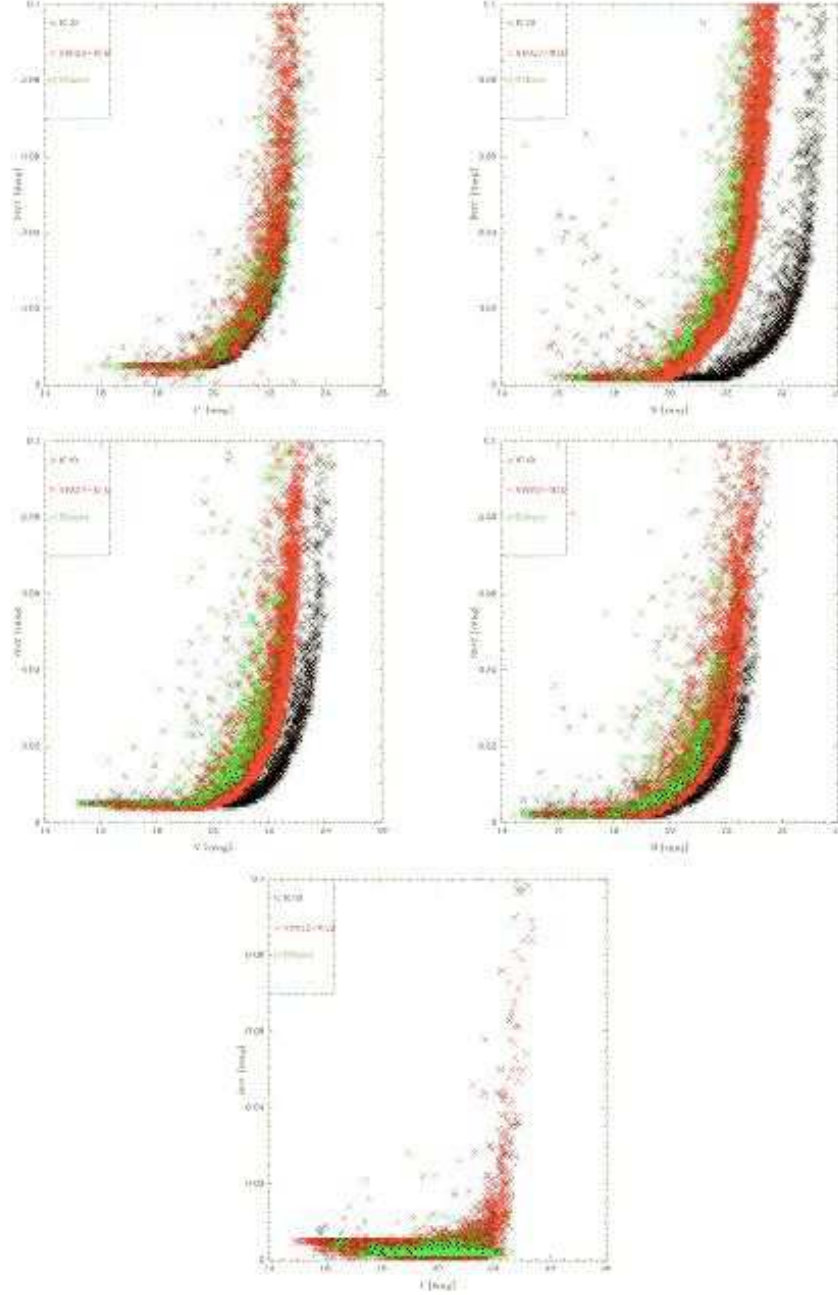


Fig. 8.— Errors as a function of magnitude. The black points are IC10, the red points are the combination of NGC 6822 and WLM, and the green points come from the other 4 galaxies. For clarity, we have plotted only every tenth point.



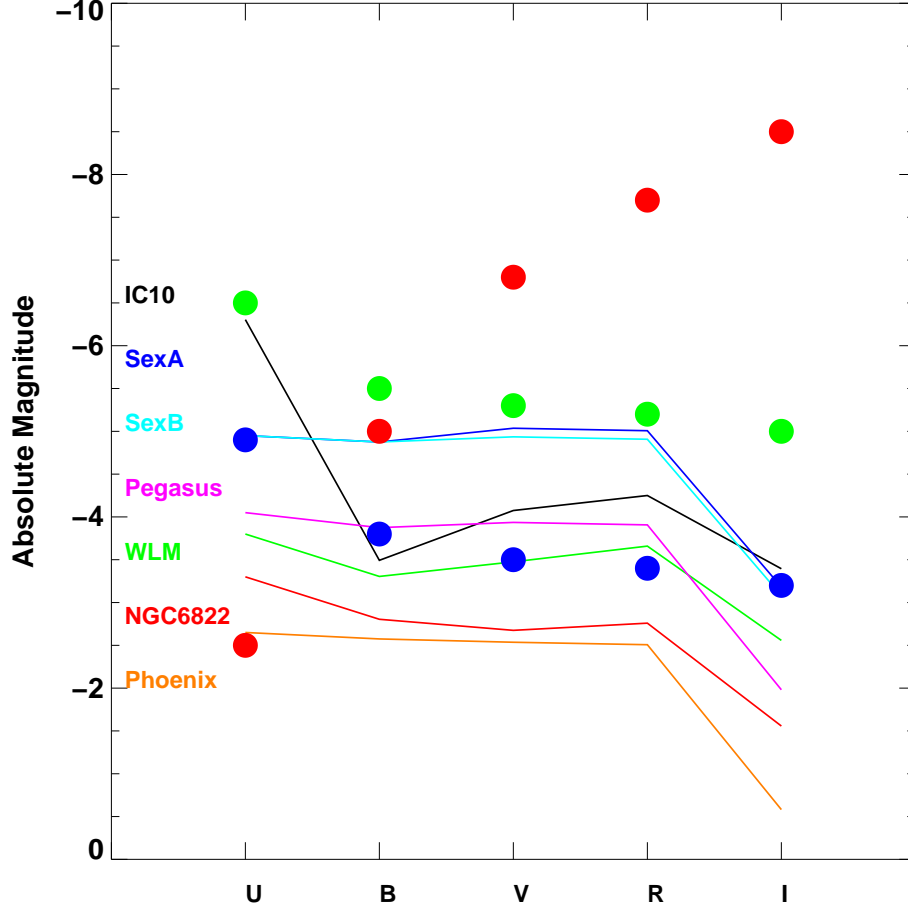


Fig. 9.— Photometric error as a function of absolute magnitude. The colored dots show the expected absolute magnitude of a  $20M_{\odot}$  star on the ZAMS (blue dots), TAMS (green dots), and as a RSG (red dots), for each of the bandpasses. The solid color curves show the 2% photometric errors actually achieved (Table 14) for each galaxy.

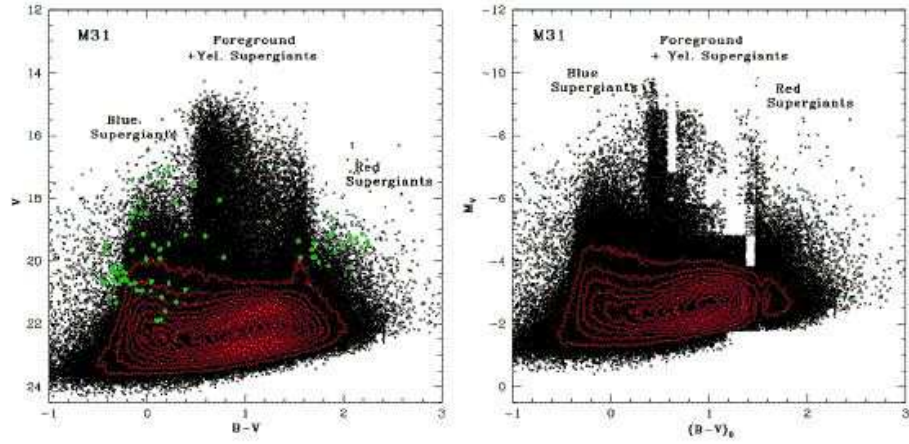


Fig. 10.— The color-magnitude diagram for M31. The data are taken from Paper I. Left: Green symbols denote spectroscopically confirmed members, from Table 8 of Paper I. Right: We show the CMD approximately “cleaned” of foreground stars (in a statistical sense) using the Bahcall & Soniera (1980) model, and converted to intrinsic color  $(B - V)_0$  and absolute visual magnitude  $M_V$ .



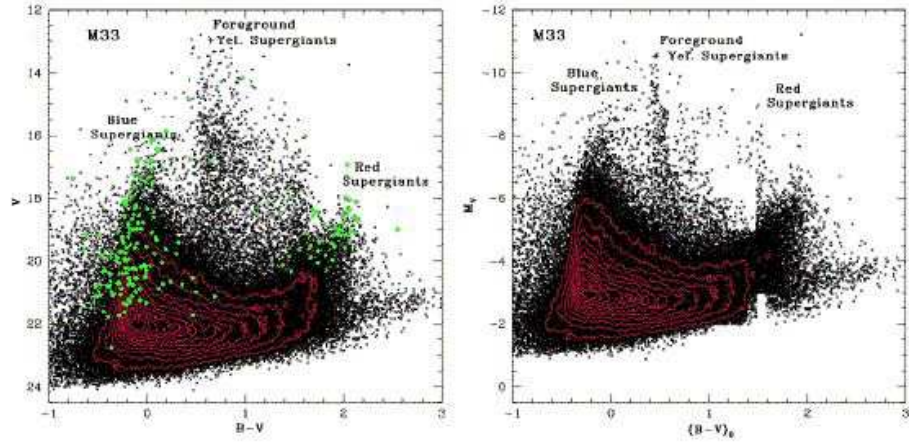


Fig. 11.— The color-magnitude diagram for M33. The data are taken from Paper I. Left: Green symbols denote spectroscopically confirmed members, from Table 9 of Paper I. Right: We show the CMD approximately “cleaned” of foreground stars (in a statistical sense) using the Bahcall & Soniera (1980) model, and converted to intrinsic color  $(B - V)_0$  and absolute visual magnitude  $M_V$ .

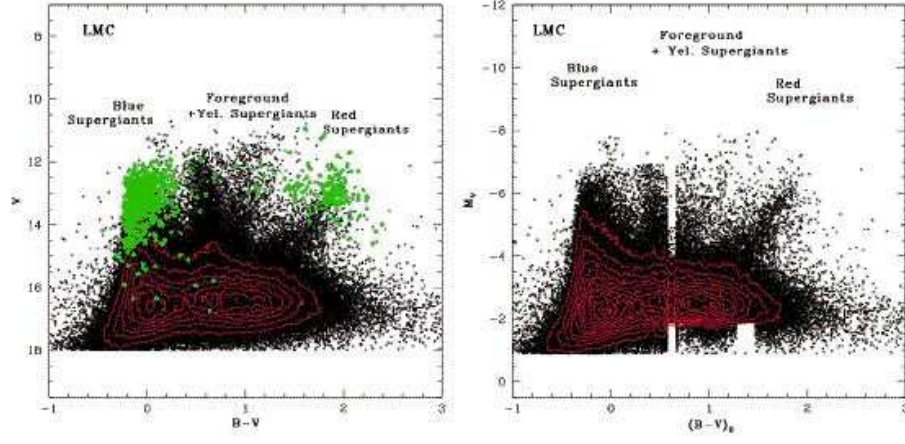


Fig. 12.— The color-magnitude diagram for the LMC. The data are taken from Massey (2002). Left: Green symbols denote spectroscopically confirmed members, taken from Table 4 of Massey (2002) and selected from Table 2 of Massey & Olsen (2003). Right: We show the CMD approximately “cleaned” of foreground stars (in a statistical sense) using the Bahcall & Soniera (1980) model, and converted to intrinsic color  $(B - V)_0$  and absolute visual magnitude  $M_V$ .

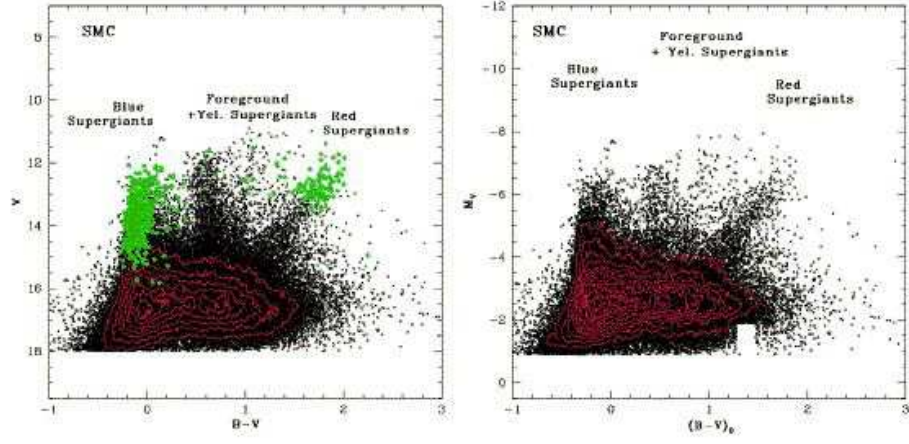


Fig. 13.— The color-magnitude diagram for SMC. The data are taken from Massey (2002). Left: Green symbols denote spectroscopically confirmed members, taken from Table 6 of Massey (2002) and selected from Table 1 of Massey & Olsen (2003). We show the CMD approximately “cleaned” of foreground stars (in a statistical sense) using the Bahcall & Soniera (1980) model, and converted to intrinsic color  $(B-V)_0$  and absolute visual magnitude  $M_V$ .

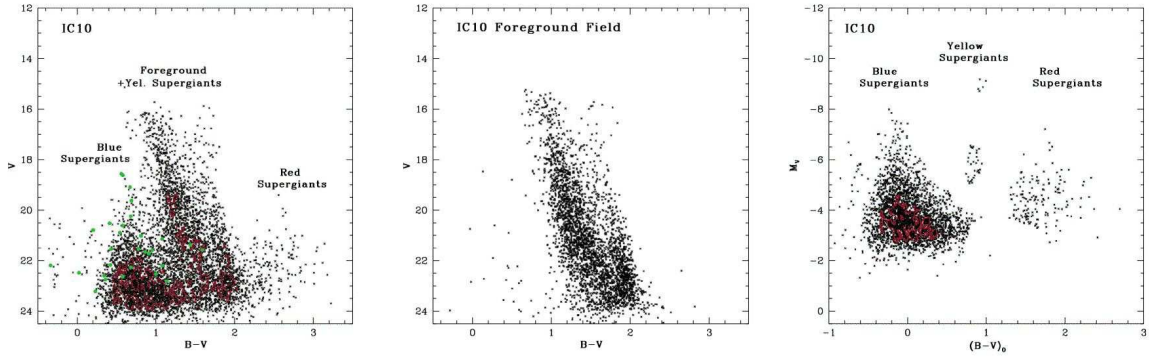


Fig. 14.— The color-magnitude diagram for IC10. Left: The CMD of the galaxy reveals a strong population of blue supergiants, as well as some red ones, but high extinction,  $E(B - V) = 0.81$ , has shifted the sequences to considerably redder colors and fainter magnitudes. To decrease the effects of foreground contamination we have restricted the sample to a region from  $\alpha_{J2000} = 00^h19^m42^s$  to  $00^h20^m55^s$ , and  $\delta_{J2000} = +59^\circ13'$  to  $+59^\circ23'$ , an area of  $0.026 \text{ deg}^2$ . Green symbols show spectroscopically confirmed members (Table 18). Middle: We show the CMD the combination of two neighboring foreground fields with the same area, chosen from the periphery of the IC10. Right: We show the CMD “cleaned” of foreground stars (in a statistical sense) and converted to intrinsic color  $(B - V)_0$  and absolute visual magnitude  $M_V$ .

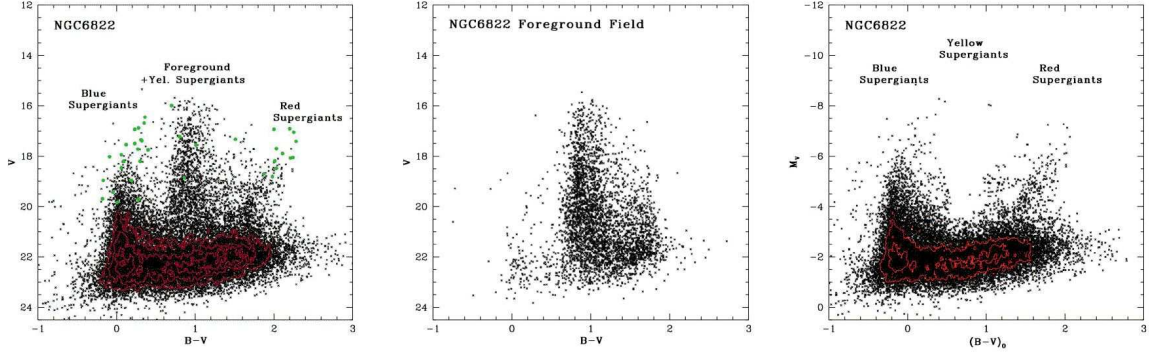


Fig. 15.— The color-magnitude diagram for NGC 6822. Left: The CMD of the galaxy reveals a strong population of blue and red supergiants, plus bright stars of intermediate color which are dominated by foreground stars. To decrease the effects of this contamination, we have restricted the sample to a region from  $\alpha_{J2000} = 19^h44^m34^s$  to  $19^h45^m22^s$ , and  $\delta_{J2000} = -14^\circ56'$  to  $-14^\circ40'$ , an area of  $0.052 \text{ deg}^2$ . Green symbols show spectroscopically confirmed members (Table 19). Middle: We show the CMD of the combination of three neighboring foreground fields with the same area, chosen from the periphery of the NGC 6822. Right: We show the CMD “cleaned” of foreground stars (in a statistical sense) and converted to intrinsic color  $(B - V)_0$  and absolute visual magnitude  $M_V$ .

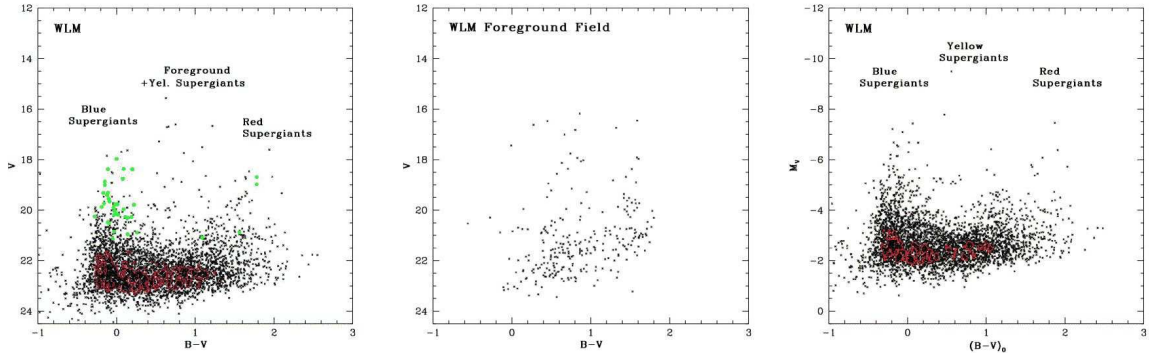


Fig. 16.— The color-magnitude diagram for WLM and neighboring foreground field. Left: The CMD of the galaxy reveals blue and red supergiants, plus a handful of bright stars of intermediate color which is dominated by foreground stars. To decrease the effects of this contamination, we have restricted the sample to a region from  $\alpha_{J2000} = 00^h01^m46^s$  to  $00^h02^m12^s$ , and  $\delta_{J2000} = -15^\circ34'$  to  $-15^\circ21'$ , an area of  $0.026 \text{ deg}^2$ . Green symbols show spectroscopically confirmed members (Table 20). Middle: We show the CMD of the combination of two neighboring foreground fields with the same area, chosen from the periphery of the Sextans B. Right: We show the CMD “cleaned” of foreground stars (in a statistical sense) and converted to intrinsic color  $(B - V)_0$  and absolute visual magnitude  $M_V$ .

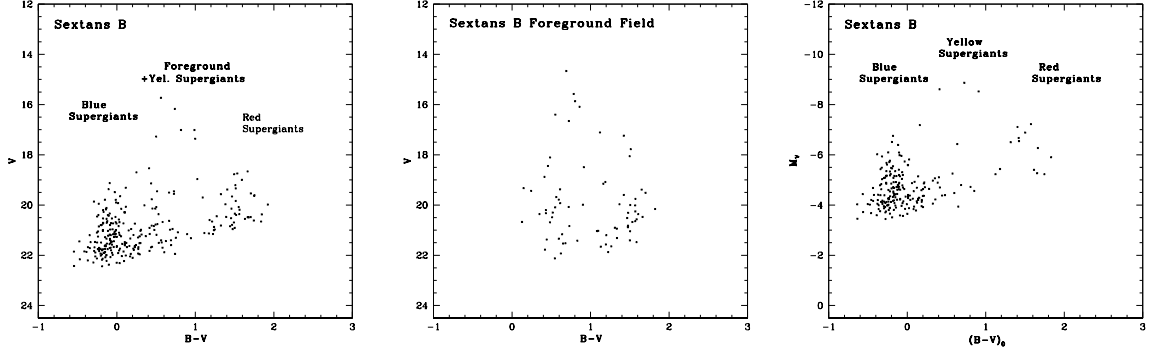


Fig. 17.— The color-magnitude diagram for Sextans B and neighboring foreground field. Left: The CMD of the galaxy reveals blue supergiants, plus a few stars of intermediate color dominated by foreground stars, plus a smattering of red stars, some of which are native to Sextans B. To decrease the effect of foreground contamination, we have restricted the same to a region from  $\alpha_{J2000} = 09^h59^m40^s$  to  $10^h00^m19^s$ , and  $\delta_{J2000} = +5^\circ17'$  to  $+5^\circ23'$ , an area of  $0.016 \text{ deg}^2$ . Middle: We show the CMD of the combination of two neighboring foreground fields with the same area, chosen from the periphery of the Sextans B. Right: We show the CMD “cleaned” of foreground stars (in a statistical sense) and converted to intrinsic color  $(B-V)_0$  and absolute visual magnitude  $M_V$ .

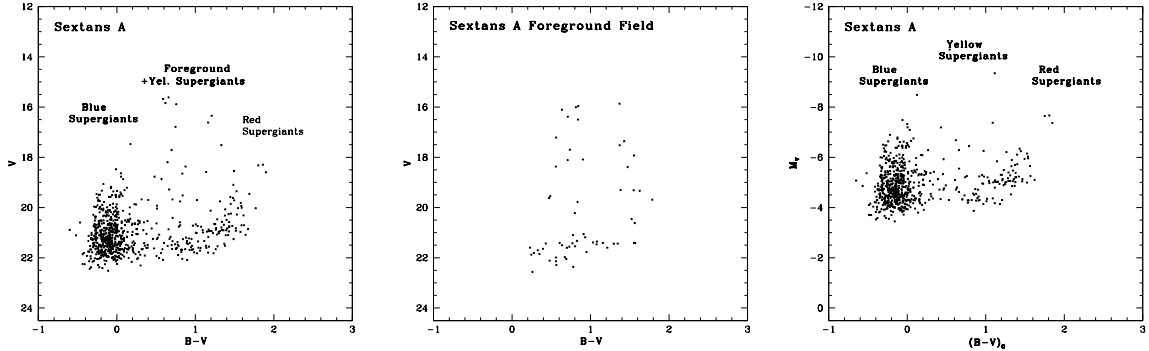


Fig. 18.— The color-magnitude diagram for Sextans A. Left: The CMD of the galaxy reveals blue supergiants, plus a few stars of intermediate color dominated by foreground stars, plus a smattering of red stars, some of which are native to Sextans A. To decrease the effect of foreground contamination, we have restricted the same to a region from  $\alpha_{J2000} = 00^h01^m46^s$  to  $00^h02^m12^s$ , and  $\delta_{J2000} = -15^\circ34'$  to  $-15^\circ21'$ , an area of  $0.016 \text{ deg}^2$ . Middle: We show the CMD of the combination of two neighboring foreground fields with the same area, chosen from the periphery of the Sextans A. Right: We show the CMD “cleaned” of foreground stars (in a statistical sense) and converted to intrinsic color  $(B-V)_0$  and absolute visual magnitude  $M_V$ .

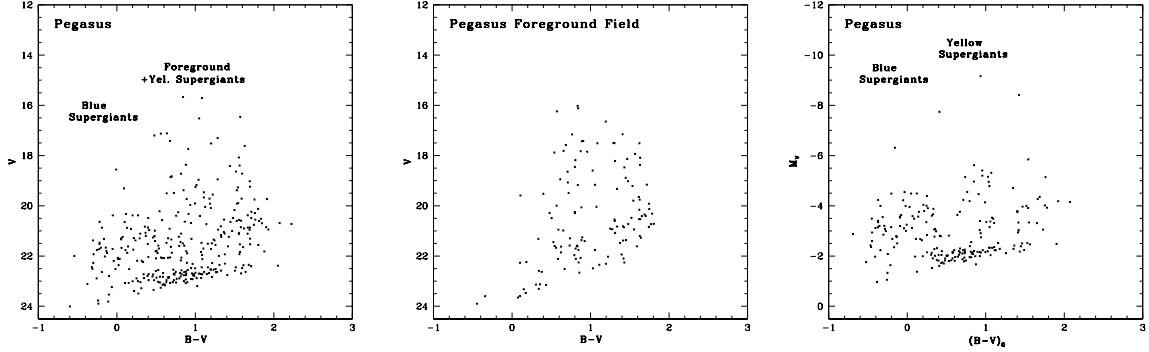


Fig. 19.— The color-magnitude diagram for Pegasus. Left: The CMD of the galaxy reveals blue supergiants, plus a few redder stars dominated by foreground stars. To decrease the effect of foreground contamination, we have restricted the same to a region from  $\alpha_{J2000} = 23^h28^m15^s$  to  $23^h28^m53^s$ , and  $\delta_{J2000} = +14^\circ41'$  to  $+14^\circ49'$ , an area of  $0.020 \text{ deg}^2$ . Middle: We show the CMD of the combination of two neighboring foreground fields with the same area, chosen from the periphery of the Pegasus dwarf. Right: We show the CMD “cleaned” of foreground stars (in a statistical sense) and converted to intrinsic color  $(B-V)_0$  and absolute visual magnitude  $M_V$ .

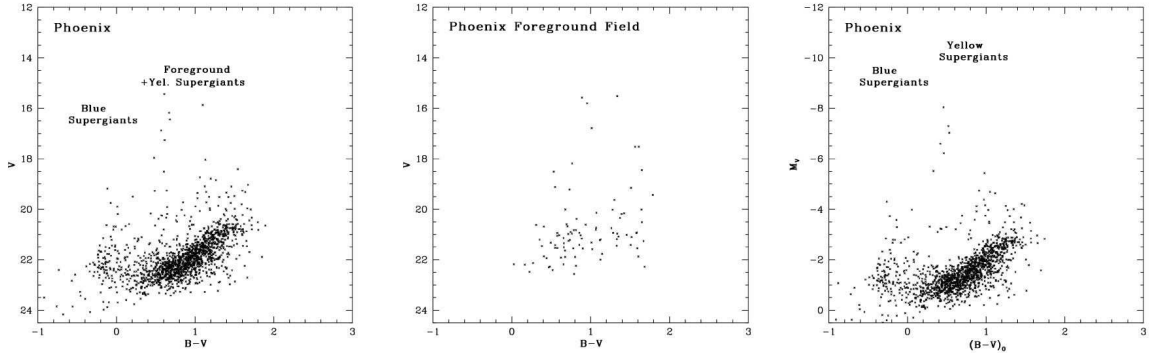


Fig. 20.— The color-magnitude diagram for Phoenix. Left: The CMD of the galaxy reveals a wealth of faint stars of intermediate and red color, and a few blue supergiants. To decrease the effect of foreground contamination, we have restricted the same to a region from  $\alpha_{J2000} = 01^h50^m42^s$  to  $01^h51^m25^s$ , and  $\delta_{J2000} = -44^\circ31'$  to  $-44^\circ23'$ , an area of  $0.017 \text{ deg}^2$ . Middle: We show the CMD of the combination of two neighboring foreground fields with the same area, chosen from the periphery of the Phoenix. Right: We show the CMD “cleaned” of foreground stars (in a statistical sense) and converted to intrinsic color  $(B-V)_0$  and absolute visual magnitude  $M_V$ .

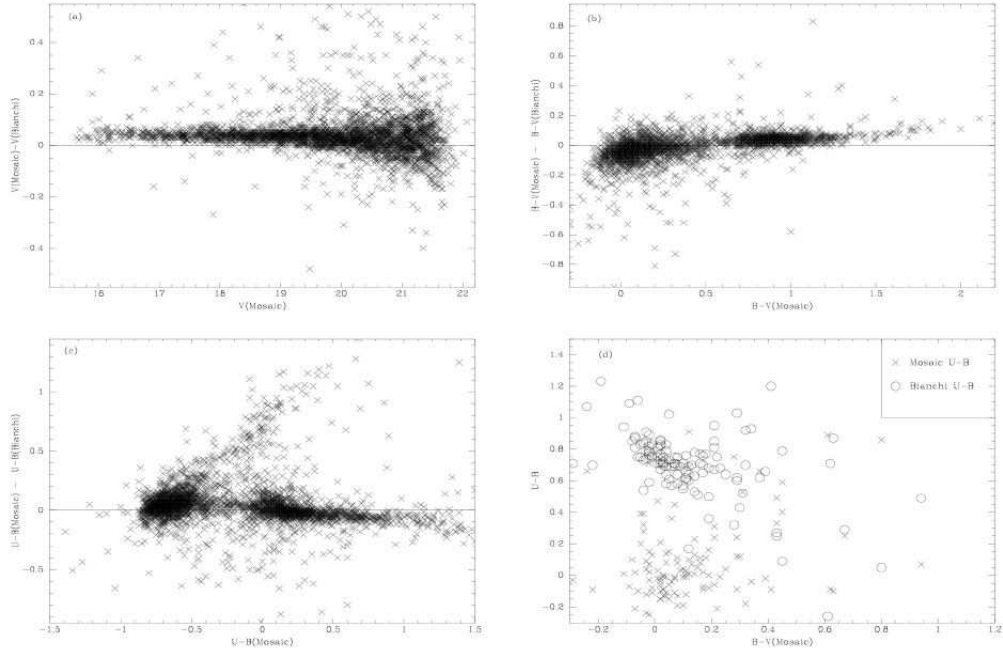


Fig. 21.— Comparison of our photometry with that of Bianchi et al. (2001). (a) There is a slight offset (0.03) mag in the  $V$  photometry. (b) The average  $B - V$  agrees, but there is a significant color term. (c) The average  $U - B$  agrees, but there is not only a color term, but a significant sequence of stars that are considerably redder Bianchi et al. (2001)’s  $U - B$  than in ours. (d) We show only those stars with  $U - B$  differences  $> 0.5$  mag from (c). For these stars the  $U - B$  photometry from Bianchi et al. (2001) (open circles) is considerably greater than that expected for their  $B - V$  colors, while that from our survey (x’s) are more in keeping with what one would expect.



Table 1. Properties of Dwarf Galaxies in Our Sample<sup>a</sup>

Galaxy	Alias	Type	$l$ [deg]	$b$ [deg]	$M_V$	$E(B - V)^b$	Dist. [Mpc]	$\log O/H+12$	$\log \dot{M}^c$	$\log \dot{M}_D^c$
IC10	UGC 192	Ir IV:	118.97	-3.34	-16.3	0.81	0.66	8.2	-1.3	-1.3
NGC 6822	...	Ir IV-V	25.34	-18.39	-16.0	0.25	0.50	8.1	-2.0	-2.0
WLM	DDO 221	Ir IV-V	75.85	-73.63	-14.4	0.07	0.93	7.7	-2.8	-2.9
Sextans B	DDO 70	IrIV-V	233.20	+43.78	-14.3	0.09	1.32	7.6	-3.0	-2.9
Sextans A	DDO 75	Ir V	246.17	+39.86	-14.2	0.05	1.45	7.5	-2.2	-1.4
Pegasus	DDO 216	Ir V	94.77	-43.55	-12.3	0.15	0.76	7.9	-4.4	-4.2
Phoenix	...	dIr/dSph	272.19	-68.95	-9.8	0.15	0.40	...	...	...
Other LG Galaxies Given for Comparison										
M31	NGC224	Sb I-II	121.17	-21.57	-21.2	0.13	0.76	9.0	-1.3 <sup>d</sup>	-3.3 <sup>d</sup>
M33	NGC598	Sc II-III	133.61	-31.33	-18.9	0.12	0.83	8.4	-1.0 <sup>d</sup>	-2.0 <sup>d</sup>
LMC	...	Ir III-IV	280.19	-33.29	-18.5	0.13	0.050	8.4	-0.8 <sup>d</sup>	-1.8 <sup>d</sup>
SMC	...	Ir IV-V	302.81	-44.33	-17.1	0.09	0.059	8.0	-1.4 <sup>d</sup>	-2.3 <sup>d</sup>

<sup>a</sup>Data from van den Bergh 2000, except as noted.

<sup>b</sup>Total  $E(B - V)$  determined in Section 3.2.

<sup>c</sup>Star formation rates (SFRs) are given in terms of  $M_\odot \text{ yr}^{-1}$  integrated over the entire galaxy ( $\log \dot{M}$ ), and also normalized by the area of the  $V$ -band scale-length (i.e.,  $\dot{M}_D$ , units of  $M_\odot \text{ yr}^{-1} \text{ kpc}^{-2}$ ); from Hunter & Elmegreen 2004, except as noted.

<sup>d</sup>Calculated here, using the  $H\alpha$  luminosities from Kennicutt & Hodge (1986) and Kennicutt et al. 1989, corrected by an additional  $A_{H\alpha} = 0.2$  mag, and adopting disk scale lengths of 5.6 kpc (M 31, Walterbos & Kennicutt 1988), 1.7 kpc (M33, Sparke & Gallagher 2000), 1.5 kpc and 0.9 kpc (LMC and SMC, Bothun & Thompson 1988).

Table 2. Mosaic Observations

Field	Obs.	Date	<i>U</i>		<i>B</i>		<i>V</i>		<i>R</i>		<i>I</i>	
			Exps.	DIQ(")	Exps.	DIQ(")	Exps.	DIQ(")	Exps.	DIQ(")	Exps.	DIQ(")
IC10 <sup>a</sup>	KPNO	2001 Sep 20-22	5x600s	1.1	5x60s, 2x900s, 1x1800s, 5x2400s	1.0	5x60s, 3x600s	0.9	5x50s, 3x200s	0.9	5x150s	0.9
NGC 6822	CTIO	2000 Sep 1-2	6x600s , 1x180s	1.2	5x120s, 1x180s	1.4	5x120s, 1x180s	1.4	5x100s, 1x180s	1.4	5x120s, 1x180s	1.0
WLM	CTIO	2000 Sep 1-2	5x600s, 1x60s	1.3	5x90s, 1x60s	1.2	5x70s, 1x60s	1.1	5x70s, 1x60s	1.0	5x200s, 1x60s	1.0
Phoenix	CTIO	2000 Sep 1	5x600s	1.3	5x60s	1.3	5x60s	1.2	5x50s	1.2	5x200s	1.0
Sextans B <sup>a</sup>	KPNO	2002 Feb 13	5x600s	1.2	5x60s	1.2	5x60s	1.2	5x50s	1.1	5x150s	0.9
Sextans A <sup>a</sup>	KPNO	2002 Feb 13	5x600s	1.4	5x60s	1.2	5x60s	1.2	5x50s	1.1	5x150s	1.1
Pegasus <sup>b</sup>	KPNO	2000 Oct 03	5x600s	1.1	5x60s	1.0	5x60s	1.0	5x50s	1.0	5x150s	0.8

<sup>a</sup>Centered on chip 2; FOV of calibrated data is 20'x30'.

<sup>b</sup>Centered in the middle, but FOV of calibrated data is 20'x30'.

Table 3. Color Terms for the CTIO 4-m Mosaic Camera<sup>a</sup>

Color Term <sup>b</sup>	Chip <sup>c</sup>							
	1	2	3	4	5	6	7	8
$K_{U1}$	−0.092	−0.047	−0.075	−0.098	−0.068	−0.044	−0.015	−0.043
$K_{U2}$	−0.272	−0.216	−0.203	−0.229	−0.210	−0.228	−0.225	−0.251
$K_B$	−0.164	−0.160	−0.130	−0.130	−0.156	−0.151	−0.171	−0.154
$K_V$	+0.006	−0.014	+0.000	+0.015	−0.009	−0.002	−0.015	+0.011
$K_R$	+0.012	−0.016	−0.008	+0.006	−0.021	+0.007	−0.034	+0.009
$K_I$	+0.027	+0.079	+0.101	+0.124	+0.054	+0.054	+0.085	+0.080

<sup>a</sup>Typical uncertainties in the color terms are 0.020.

<sup>b</sup>The color terms are defined as follows:

$$u_{\text{Mosaic}} = K_{U1}(U - B)_{\text{std}} + C_U, (U - B)_{\text{std}} > 0$$

$$u_{\text{Mosaic}} = K_{U2}(U - B)_{\text{std}} + C_U, (U - B)_{\text{std}} < 0$$

$$b_{\text{Mosaic}} = K_B(B - V)_{\text{std}} + C_B$$

$$v_{\text{Mosaic}} = K_V(B - V)_{\text{std}} + C_V$$

$$r_{\text{Mosaic}} = K_R(V - R)_{\text{std}} + C_R$$

$$i_{\text{Mosaic}} = K_I(R - I)_{\text{std}} + C_I,$$

where the  $K$ 's are the color terms, and  $C$ 's are the zero-points.

<sup>c</sup>Numbered as in the Mosaic II manual (Schommer et al. 2000), starting with the south-western chip and continuing north along the western set of four, and then north along the eastern four.

Table 4. Average Agreement Between Different Calibrations<sup>a</sup>

Index	NGC 6822				WLM			
	Lowell 1.1-m		CTIO 0.9-m		Lowell 1.1-m		CTIO 0.9-m	
	#	Diff	#	Diff	#	Diff	#	Diff.
V	133	+0.016	165	−0.005	20	−0.005	35	−0.002
B−V	133	+0.020	165	−0.021	20	−0.005	35	−0.001
U−B	130	−0.037	164	−0.004	20	−0.028	34	+0.018
V−R	132	+0.008	164	0.000	20	−0.008	35	−0.010
R−I	69	+0.016	95	−0.003	12	+0.014	27	−0.001

<sup>a</sup>We give the median differences between the final calibrated photometry and that of the Lowell 1.1-m and CTIO 0.9-m calibration data for NGC 6822 and WLM.

Table 5. IC10 Catalog

LGGS	$\alpha_{2000}$	$\delta_{2000}$	$V$	$\sigma_V$	$B - V$	$\sigma_{B-V}$	$U - B$	$\sigma_{U-B}$	$V - R$	$\sigma_{V-R}$	$R - I$	$\sigma_{R-I}$	$N_V$	$N_B$	$N_U$	$N_R$	$N_I$	Sp. Type	Ref.
J001908.25+592855.5	00 19 08.25	+59 28 55.5	20.550	0.021	1.375	0.049	0.547	0.104	0.864	0.024	0.976	0.012	1	1	1	1	1		
J001908.27+593126.8	00 19 08.27	+59 31 26.8	18.556	0.008	1.358	0.015	0.750	0.024	0.827	0.009	0.882	0.005	1	1	1	1	1		
J001908.30+592050.7	00 19 08.30	+59 20 50.7	18.509	0.009	1.224	0.014	0.683	0.022	0.766	0.010	0.752	0.005	1	1	1	1	1		
J001908.32+590945.5	00 19 08.32	+59 09 45.5	18.531	0.008	1.289	0.014	0.567	0.017	0.858	0.010	0.841	0.006	1	1	1	1	1		
J001908.33+591514.9	00 19 08.33	+59 15 14.9	19.151	0.008	1.042	0.015	0.435	0.022	0.730	0.010	0.715	0.006	1	1	1	1	1		

Note. — Notes—Units of right ascension are hours, minutes, and seconds, and units of declination are degrees, arcminutes, and arcseconds. Note that an entry of “99.999” denotes no measurement. Table 5 is published in its entirety in the electronic edition of the *Astronomical Journal*. A portion is shown here for guidance regarding its form and content.

References. — For spectral types: (1) Massey et al. 1992; (2) Massey & Armandroff 1995; (3) Massey & Holmes 2002; (4) Crowther et al. 2003.

Table 6. NGC 6822 Catalog

LGGS	$\alpha_{2000}$	$\delta_{2000}$	$V$	$\sigma_V$	$B - V$	$\sigma_{B-V}$	$U - B$	$\sigma_{U-B}$	$V - R$	$\sigma_{V-R}$	$R - I$	$\sigma_{R-I}$	$N_V$	$N_B$	$N_U$	$N_R$	$N_I$	Sp. Type	Ref.
J194335.94-145605.5	19 43 35.94	-14 56 05.5	21.023	0.028	1.247	0.056	99.999	99.999	0.827	0.041	0.818	0.030	1	1	0	1	1		
J194335.95-145043.5	19 43 35.95	-14 50 43.5	21.733	0.072	1.126	0.106	99.999	99.999	0.578	0.091	0.779	0.056	1	1	0	1	1		
J194336.01-150039.3	19 43 36.01	-15 00 39.3	21.683	0.038	1.023	0.081	99.999	99.999	0.544	0.064	0.552	0.052	1	1	0	1	1		
J194336.03-145851.2	19 43 36.03	-14 58 51.2	19.199	0.008	1.544	0.020	99.999	99.999	0.995	0.010	1.030	0.006	1	1	0	1	1		
J194336.04-150013.7	19 43 36.04	-15 00 13.7	21.102	0.030	1.264	0.047	99.999	99.999	0.809	0.039	0.683	0.025	1	1	0	1	1		

Note. — Notes—Units of right ascension are hours, minutes, and seconds, and units of declination are degrees, arcminutes, and arcseconds. Note that an entry of “99.999” denotes no measurement. Table 6 is published in its entirety in the electronic edition of the *Astronomical Journal*. A portion is shown here for guidance regarding its form and content.

References. — For spectral types: (1) Massey et al. 1995a; (2) Massey & Johnson 1998; (3) Muschiolok et al. 1999; (4) Venn et al. 2001; (5) Humphreys 1980a; (6) Massey 1998b.

Table 7. WLM Catalog

LGGS	$\alpha_{2000}$	$\delta_{2000}$	$V$	$\sigma_V$	$B - V$	$\sigma_{B-V}$	$U - B$	$\sigma_{U-B}$	$V - R$	$\sigma_{V-R}$	$R - I$	$\sigma_{R-I}$	$N_V$	$N_B$	$N_U$	$N_R$	$N_I$	Sp. Type	Ref.
J000044.71-153324.4	00 00 44.71	-15 33 24.4	21.254	0.032	1.780	0.114	99.999	99.999	0.962	0.042	99.999	99.999	1	1	0	1	0		
J000044.81-152808.8	00 00 44.81	-15 28 08.8	20.696	0.018	1.395	0.050	99.999	99.999	0.904	0.022	99.999	99.999	1	1	0	1	0		
J000045.04-152842.2	00 00 45.04	-15 28 42.2	19.982	0.012	1.317	0.031	1.210	0.113	0.836	0.013	99.999	99.999	1	1	1	1	0		
J000045.06-152246.1	00 00 45.06	-15 22 46.1	21.754	0.061	0.529	0.089	-0.853	0.085	0.555	0.082	99.999	99.999	1	1	1	1	0		
J000045.20-151944.4	00 00 45.20	-15 19 44.4	20.223	0.015	1.498	0.035	99.999	99.999	1.208	0.017	1.625	0.009	1	1	0	1	1		

Note. — Notes—Units of right ascension are hours, minutes, and seconds, and units of declination are degrees, arcminutes, and arcseconds. Note that an entry of “99.999” denotes no measurement. Table 7 is published in its entirety in the electronic edition of the *Astronomical Journal*. A portion is shown here for guidance regarding its form and content.

References. — For spectral types: (1) Bresolin et al. 2006

Table 8. Sextans B Catalog

LGGS	$\alpha_{2000}$	$\delta_{2000}$	$V$	$\sigma_V$	$B - V$	$\sigma_{B-V}$	$U - B$	$\sigma_{U-B}$	$V - R$	$\sigma_{V-R}$	$R - I$	$\sigma_{R-I}$	$N_V$	$N_B$	$N_U$	$N_R$	$N_I$
J095922.35+051211.7	09 59 22.35	+05 12 11.7	18.184	0.008	0.571	0.013	-0.111	0.014	0.370	0.009	0.352	0.005	1	1	1	1	1
J095922.44+051221.6	09 59 22.44	+05 12 21.6	19.964	0.023	1.526	0.053	1.223	0.156	0.979	0.025	0.942	0.010	1	1	1	1	1
J095922.83+052943.4	09 59 22.83	+05 29 43.4	18.091	0.008	0.668	0.011	-0.041	0.010	0.402	0.011	0.388	0.007	1	1	1	1	1
J095922.88+053137.8	09 59 22.88	+05 31 37.8	20.932	0.060	0.995	0.104	0.659	0.141	0.556	0.070	0.513	0.036	1	1	1	1	1
J095922.92+051001.3	09 59 22.92	+05 10 01.3	20.020	0.031	0.516	0.043	-0.272	0.035	0.297	0.037	0.342	0.020	1	1	2	1	1

Note. — Notes—Units of right ascension are hours, minutes, and seconds, and units of declination are degrees, arcminutes, and arcseconds. Note that an entry of “99.999” denotes no measurement. Table 8 is published in its entirety in the electronic edition of the *Astronomical Journal*. A portion is shown here for guidance regarding its form and content.



Table 9. Sextans A Catalog

LGGS	$\alpha_{2000}$	$\delta_{2000}$	$V$	$\sigma_V$	$B - V$	$\sigma_{B-V}$	$U - B$	$\sigma_{U-B}$	$V - R$	$\sigma_{V-R}$	$R - I$	$\sigma_{R-I}$	$N_V$	$N_B$	$N_U$	$N_R$	$N_I$
J101021.29-045018.6	10 10 21.29	-04 50 18.6	16.003	0.005	0.848	0.007	99.999	99.999	0.511	0.007	99.999	99.999	1	1	0	1	0
J101021.41-044609.4	10 10 21.41	-04 46 09.4	21.256	0.055	1.077	0.097	99.999	99.999	0.857	0.062	0.714	0.029	1	1	0	1	1
J101021.68-045246.3	10 10 21.68	-04 52 46.3	21.051	0.047	1.310	0.092	99.999	99.999	0.640	0.056	0.645	0.030	1	1	0	1	1
J101022.48-044503.1	10 10 22.48	-04 45 03.1	19.404	0.014	1.523	0.033	1.145	0.082	1.028	0.016	1.349	0.008	1	1	1	1	2
J101022.50-044124.1	10 10 22.50	-04 41 24.1	19.982	0.017	0.292	0.025	99.999	99.999	0.461	0.027	0.447	0.021	1	1	0	1	2

Note. — Notes—Units of right ascension are hours, minutes, and seconds, and units of declination are degrees, arcminutes, and arcseconds. Note that an entry of “99.999” denotes no measurement. Table 9 is published in its entirety in the electronic edition of the *Astronomical Journal*. A portion is shown here for guidance regarding its form and content.

Table 10. Pegasus Catalog

LGGS	$\alpha_{2000}$	$\delta_{2000}$	$V$	$\sigma_V$	$B - V$	$\sigma_{B-V}$	$U - B$	$\sigma_{U-B}$	$V - R$	$\sigma_{V-R}$	$R - I$	$\sigma_{R-I}$	$N_V$	$N_B$	$N_U$	$N_R$	$N_I$
J232720.15+145207.4	23 27 20.15	+14 52 07.4	16.059	0.005	0.761	0.009	0.180	0.009	0.415	0.007	99.999	99.999	1	1	1	1	0
J232720.23+144410.7	23 27 20.23	+14 44 10.7	22.169	0.103	1.101	0.305	99.999	99.999	1.200	0.114	1.626	0.048	1	1	0	1	1
J232720.51+145345.6	23 27 20.51	+14 53 45.6	19.042	0.011	1.504	0.025	1.133	0.066	0.929	0.014	0.959	0.008	1	1	1	1	1
J232720.56+143751.6	23 27 20.56	+14 37 51.6	16.467	0.006	0.892	0.008	0.423	0.007	0.502	0.008	99.999	99.999	1	1	1	1	0
J232720.77+145120.1	23 27 20.77	+14 51 20.1	21.109	0.033	1.522	0.089	99.999	99.999	0.896	0.040	0.931	0.023	1	1	0	1	1

Note. — Notes—Units of right ascension are hours, minutes, and seconds, and units of declination are degrees, arcminutes, and arcseconds. Note that an entry of “99.999” denotes no measurement. Table 10 is published in its entirety in the electronic edition of the *Astronomical Journal*. A portion is shown here for guidance regarding its form and content.

Table 11. Phoenix Catalog

LGGS	$\alpha_{2000}$	$\delta_{2000}$	$V$	$\sigma_V$	$B - V$	$\sigma_{B-V}$	$U - B$	$\sigma_{U-B}$	$V - R$	$\sigma_{V-R}$	$R - I$	$\sigma_{R-I}$	$N_V$	$N_B$	$N_U$	$N_R$	$N_I$
J014928.54-443314.7	01 49 28.54	-44 33 14.7	22.089	0.084	0.254	0.109	0.470	0.110	0.452	0.107	0.238	0.066	1	1	1	1	1
J014929.04-443519.3	01 49 29.04	-44 35 19.3	20.630	0.021	1.604	0.065	99.999	99.999	1.268	0.022	1.670	0.008	1	1	0	1	1
J014929.69-442318.7	01 49 29.69	-44 23 18.7	18.499	0.007	1.402	0.019	0.970	0.026	0.960	0.009	0.990	0.006	1	1	1	1	1
J014929.70-443119.8	01 49 29.70	-44 31 19.8	18.128	0.006	1.105	0.014	1.286	0.018	0.716	0.008	0.662	0.005	1	1	1	1	1
J014929.74-443600.8	01 49 29.74	-44 36 00.8	18.356	0.006	0.687	0.011	0.163	0.011	0.376	0.009	0.412	0.007	1	1	1	1	1

Note. — Notes—Units of right ascension are hours, minutes, and seconds, and units of declination are degrees, arcminutes, and arcseconds. Note that an entry of “99.999” denotes no measurement. Table 11 is published in its entirety in the electronic edition of the *Astronomical Journal*. A portion is shown here for guidance regarding its form and content.

Table 12. Revised M31 Catalog

LGGS	$\alpha_{2000}$	$\delta_{2000}$	$V$	$\sigma_V$	$B - V$	$\sigma_{B-V}$	$U - B$	$\sigma_{U-B}$	$V - R$	$\sigma_{V-R}$	$R - I$	$\sigma_{R-I}$	$N_V$	$N_B$	$N_U$	$N_R$	$N_I$	Sp. Type	Ref.
J003701.92+401233.2	00 37 1.92	+40 12 33.2	19.862	0.017	-0.021	0.021	-0.928	0.015	0.204	0.023	99.999	99.999	1	2	1	1	0		
J003701.93+401218.4	00 37 1.93	+40 12 18.4	18.739	0.008	1.494	0.015	0.945	0.036	0.946	0.014	99.999	99.999	1	2	1	1	0		
J003702.03+401141.4	00 37 2.03	+40 11 41.4	21.225	0.043	1.362	0.085	99.999	99.999	0.748	0.049	0.694	0.024	1	1	0	1	1		
J003702.05+400633.5	00 37 2.05	+40 06 33.5	21.091	0.044	0.050	0.061	-1.110	0.052	0.042	0.074	99.999	99.999	1	2	1	1	0		
J003702.13+400945.6	00 37 2.13	+40 09 45.6	16.091	0.006	1.287	0.007	0.983	0.007	0.792	0.010	99.999	99.999	1	2	1	1	0		

Note. — Notes—Units of right ascension are hours, minutes, and seconds, and units of declination are degrees, arcminutes, and arcseconds. Note that an entry of “99.999” denotes no measurement. Table 5 is published in its entirety in the electronic edition of the *Astronomical Journal*. A portion is shown here for guidance regarding its form and content.

References. — For spectral types: (1) Paper I; (2) Trundle et al. 2002; (3) Humphreys 1979; (4) Massey et al. 1995a; (5) Massey et al. 1986; (6) Humphreys et al. 1990; (7) Bianchi et al. 1994; (8) P. Massey, 1996-2006, unpublished; (9) Hubble & Sandage 1953; (10) Humphreys et al. 1988; (11) Massey 1998b; (12) Massey & Johnson 1998 and references therein.

Table 13. Revised M33 Catalog

LGGS	$\alpha_{2000}$	$\delta_{2000}$	$V$	$\sigma_V$	$B - V$	$\sigma_{B-V}$	$U - B$	$\sigma_{U-B}$	$V - R$	$\sigma_{V-R}$	$R - I$	$\sigma_{R-I}$	$N_V$	$N_B$	$N_U$	$N_R$	$N_I$	Sp. Type	Ref.
J013146.16+301855.6	01 31 46.16	+30 18 55.6	19.555	0.013	1.533	0.025	1.141	0.047	1.030	0.015	99.999	99.999	1	1	1	1	0		
J013146.18+302932.4	01 31 46.18	+30 29 32.4	20.560	0.068	0.645	0.117	99.999	99.999	0.564	0.115	99.999	99.999	1	1	0	1	0		
J013146.18+302931.4	01 31 46.18	+30 29 31.4	21.027	0.061	0.090	0.113	0.266	0.118	1.012	0.111	99.999	99.999	1	1	1	1	0		
J013146.20+302706.2	01 31 46.20	+30 27 6.2	21.057	0.032	1.857	0.084	99.999	99.999	0.924	0.036	99.999	99.999	1	1	0	1	0		
J013146.21+302026.9	01 31 46.21	+30 20 26.9	21.179	0.038	0.962	0.066	0.749	0.096	0.588	0.047	99.999	99.999	1	1	1	1	0		

Note. — Notes—Units of right ascension are hours, minutes, and seconds, and units of declination are degrees, arcminutes, and arcseconds. Note that an entry of “99.999” denotes no measurement. Table 5 is published in its entirety in the electronic edition of the *Astronomical Journal*. A portion is shown here for guidance regarding its form and content.

References. — For spectral types: (1) Humphreys 1980b; (2) Massey et al. 1996; (3) Massey et al. 1995a; (4) P. Massey 1996-2006, unpublished; (5) Monteverde et al. 1996; (6) Hubble & Sandage 1953; (7) van den Bergh et al. 1975; (8) Massey et al. 1998b; (9) Massey & Johnson 1998 and references therein.

Table 14. Median Errors

[illegible]

Table 15. Brightness of a  $20M_{\odot}$  Star

Stage <sup>a</sup>	<i>U</i>	<i>B</i>	<i>V</i>	<i>R</i>	<i>I</i>
IC10					
ZAMS (9.5 V)	23.2	23.8	23.2	22.8	22.5
TAMS (B1 I)	21.6	22.1	21.4	21.0	20.7
RSG	25.6	22.6	19.9	18.5	17.2
NGC 6822					
ZAMS (O9.5 V)	19.8	20.8	20.8	20.7	20.8
TAMS (B1 I)	18.2	19.1	19.0	18.9	19.0
RSG	22.2	19.6	17.5	16.4	15.5
WLM					
ZAMS (O9.5 V)	20.3	21.3	21.6	21.6	21.8
TAMS (B1 I)	18.7	19.6	19.8	19.8	20.0
RSG	22.7	20.1	18.3	17.3	16.5
Sextans B					
ZAMS (O9.5 V)	21.2	22.2	22.4	22.4	22.6
TAMS (B1 I) 19.6	20.5	20.6	20.6	20.8	
RSG	23.6	21.0	19.1	18.1	17.3
Sextans A					
ZAMS (O9.5 V)	21.2	22.2	22.5	22.5	22.7
TAMS (B1 I)	19.6	20.5	20.7	20.7	20.9
RSG	23.6	21.0	19.2	18.2	17.4
Pegasus					
ZAMS (O9.5 V)	20.3	21.2	21.4	21.4	21.5
TAMS (B1 I)	18.7	19.5	19.6	19.6	19.7
RSG	22.7	20.0	18.1	17.1	16.2
Phoenix					
ZAMS (O9.5 V)	18.9	19.9	20.0	20.0	20.1
TAMS (B1 I)	17.3	18.2	18.2	18.2	18.3
RSG	21.3	18.7	16.7	15.7	14.8
M31					
ZAMS (O9.5 V)	20.2	21.2	21.3	21.3	21.5
TAMS (B1 I)	18.6	19.5	19.5	19.5	19.7
RSG	22.6	20.0	18.0	17.0	16.2
M33					
ZAMS (O9.5 V)	20.3	21.3	21.5	21.5	21.6
TAMS (B1 I)	18.7	19.6	19.7	19.7	19.8
RSG	22.7	20.1	18.2	17.2	16.3
LMC					
ZAMS (O9.5 V)	9.2	10.3	10.4	10.4	10.6
TAMS (B1 I)	7.6	8.6	8.6	8.6	8.8
RSG	11.6	9.1	7.1	6.1	5.3
SMC					
ZAMS (O9.5 V)	9.0	10.1	10.4	10.5	10.7
TAMS (B1 I)	7.4	8.4	8.6	8.7	8.9
RSG	11.4	8.9	7.1	6.2	5.4

<sup>a</sup>A  $20M_{\odot}$  zero-age main sequence (ZAMS) star taken to be 09.5 V with  $M_V = -3.5$ , and  $(U - B)_0 = -1.1$ ,  $(B - V)_0 = -0.3$ ,  $V - R = -0.1$ , and  $(R - I)_0 = -0.2$ . A  $20M_{\odot}$  terminal-age main sequence (TAMS) star taken to be B1 I with  $M_V = -5.3$ ,  $(U - B)_0 = -1.0$ ,  $(B - V) = -0.2$ ,  $(V - R)_0 = -0.1$ , and  $(R - I)_0 = -0.2$ . A  $20M_{\odot}$  RSG is assumed to have  $M_V = -6.8$ , and  $(U - B)_0 = +2.5$ ,  $(B - V)_0 = +1.8$ ,  $(V - R)_0 = +0.9$ ,  $(R - I)_0 = +0.8$ .



Table 16. Foreground Contribution to Selected Portions of the CMDs

Galaxy	Selection Criteria		Area (deg <sup>2</sup> )	Foreground (%)	Relative Contributions (%)		
	$V$ Range	$B - V$ Range			Disk dwarfs	Halo dwarfs	Halo giants
M31	15-20	0.4-1.1	2.2	50	86	7	7
M31	16-20	1.2-1.8	2.2	85	100	0	0
M33	15-20	0.4-1.1	0.8	40	73	15	12
M33	16-20	1.2-1.8	0.8	70	99	1	0
LMC	11-15	0.4-1.1	14.5	54	85	9	6
SMC	11-15	0.4-1.1	7.2	45	82	6	12
IC10	16-20	0.5-2.0	0.026	100	100	0	0
NGC 6822	16-20	0.5-1.4	0.052	94	68	12	20
WLM	16-20	0.4-1.0	0.023	95	11	55	34
WLM	16-20	1.1-1.9	0.023	74	97	3	0
Sextans B	16-20	0.4-1.1	0.016	85	42	34	24
Sextans A	16-20	0.4-1.1	0.016	85	47	30	23
Pegasus	16-20	0.4-1.9	0.020	48	69	18	13
Phoenix	16-20	0.4-1.9	0.017	30	52	30	18

Table 17. Reddenings

Galaxy	Total $E(B - V)$	Foreground $E(B - V)^a$	Internal $E(B - V)$
M31	$0.13 \pm 0.02$	0.06	0.07
M33	$0.12 \pm 0.02$	0.05	0.07
LMC	$0.13^b$	0.08	0.05
SMC	$0.09^b$	0.04	0.05
IC10	$0.81 \pm 0.02$	0.7-1.3	...
NGC 6822	$0.25 \pm 0.02$	0.22	0.03
WLM	$0.07 \pm 0.05$	0.03	0.04
Sextans B	$0.09 \pm 0.05$	0.03	0.06
Sextans A	$0.05 \pm 0.05$	0.04	0.01
Pegasus	$0.15 \pm 0.05$	0.06	0.09
Phoenix	$0.15 \pm 0.05$	0.02	0.13

<sup>a</sup>Calculated from the Schlegel et al. 1998  $100\mu\text{m}$  dust emission maps, using software kindly made publicly available by D. Schlegel and D. Finkbeiner, via <http://astro.berkeley.edu/davis/dust/local/local/html>. The estimates for the foreground reddening towards M31, the LMC, and SMC come directly from their web site.

<sup>b</sup>Adopted from Massey et al. 1995b.

Table 18. IC10 Members Confirmed by Spectroscopy

LGGS	$\alpha_{2000}$	$\delta_{2000}$	$V$	$B - V$	$U - B$	$V - R$	$R - I$	Sp. Type	Notes <sup>a</sup>	Cross-ID <sup>b</sup>	Ref.
J001956.99+591707.5	00 19 56.99	+59 17 07.5	21.47	0.64	-0.37	0.42	0.34	WC4-5+abs		[MAC92] 1	2,4
J001959.63+591654.7	00 19 59.63	+59 16 54.7	21.02	0.81	-0.29	0.53	0.53	WC4	M	[MAC92] 2	1,4
J001959.69+591654.9	00 19 59.69	+59 16 54.9	21.58	1.59	-2.10	1.04	0.56	WC4	M	[MAC92] 2	1,4
J002003.01+591827.0	00 20 03.01	+59 18 27.0	22.20	1.08	99.99	0.82	0.79	WC4		RSMV6	4
J002004.25+591806.2	00 20 04.25	+59 18 06.2	21.66	0.86	-0.27	0.56	0.57	WC4-5+abs		RSMV5	4
J002011.55+591857.9	00 20 11.55	+59 18 57.9	19.62	0.69	-0.39	0.50	0.51	WC4-5		[MAC92] 4	2,4
J002012.84+592008.1	00 20 12.84	+59 20 08.1	21.59	0.95	-0.30	0.44	-0.11	WNE/C4		[MAC92] 5	2,4
J002020.31+591839.5	00 20 20.31	+59 18 39.5	21.54	0.43	-0.11	0.70	0.69	WNE+abs	M	RSMV9	4
J002020.34+591840.1	00 20 20.34	+59 18 40.1	22.19	-0.34	0.04	1.31	0.72	WNE+abs	M	RSMV9	4
J002020.56+591837.3	00 20 20.56	+59 18 37.3	20.24	0.68	-0.54	0.61	0.45	WN10		RSMV8	4
J002021.87+591741.1	00 20 21.87	+59 17 41.1	19.09	0.67	-0.63	0.45	0.45	WC4-5+abs	M	[MAC92] 7	2,4
J002021.97+591741.2	00 20 21.97	+59 17 41.2	20.79	0.20	0.46	0.49	0.14	WC4-5+abs	M	[MAC92] 7	2,4
J002022.68+591846.8	00 20 22.68	+59 18 46.8	23.22	0.23	99.99	0.56	99.99	WN3		[MAC92] 9	2,4
J002022.76+591753.4	00 20 22.76	+59 17 53.4	22.82	1.14	99.99	0.67	1.23	WC4		RSMV11	4
J002023.35+591742.2	00 20 23.35	+59 17 42.2	20.52	0.41	0.32	0.48	0.10	WC7		[MAC92] 10	2,4
J002025.70+591648.3	00 20 25.70	+59 16 48.3	22.53	1.00	99.99	0.60	0.62	WNE		RSMV12	4
J002026.20+591726.3	00 20 26.18	+59 17 26.3	21.15	1.08	-0.46	0.96	1.34	WC4		[MAC92] 12	2,4
J002026.54+591705.0	00 20 26.54	+59 17 05.0	22.63	0.58	99.99	0.89	-0.48	WC4		RSMV10	4
J002026.69+591732.8	00 20 26.69	+59 17 32.8	20.89	0.54	-0.48	0.55	0.62	WC5-6		[MAC92] 13	2,4
J002026.94+591719.9	00 20 26.94	+59 17 19.9	20.61	0.58	-0.01	0.64	0.90	WC5-6		[MAC92] 14	2,4
J002027.02+591818.0	00 20 27.02	+59 18 18.0	22.27	0.68	99.99	0.58	0.55	WC6-7		[MAC92] 15	2
J002027.73+591737.3	00 20 27.73	+59 17 37.3	18.56	0.56	-0.11	0.37	0.34	WN	M	[MAC92] 24	3
J002027.75+591738.1	00 20 27.75	+59 17 38.1	18.62	0.58	-0.22	0.47	0.38	WN	M	[MAC92] 24	3
J002028.07+591714.3	00 20 28.07	+59 17 14.3	21.54	0.78	-0.26	0.70	0.71	WN7-8		RSMV2	4
J002029.08+591651.7	00 20 29.08	+59 16 51.7	21.72	0.91	-1.09	0.14	0.75	WNE+OB	M	[MAC92] 17	2,4
J002029.12+591651.8	00 20 29.12	+59 16 51.8	22.48	0.02	-0.92	0.85	0.81	WNE+OB	M	[MAC92] 17	2,4
J002031.05+591904.2	00 20 31.05	+59 19 04.2	22.60	0.34	99.99	0.56	0.34	WN4		[MAC92] 19	1,4
J002032.80+591716.4	00 20 32.80	+59 17 16.4	21.38	1.44	99.99	1.29	1.42	WN7-8		[MAC92] 23	3
J002034.52+591714.6	00 20 34.52	+59 17 14.6	22.17	0.42	0.29	0.59	0.49	WC5		[MAC92] 20	1,4
J002041.61+591624.8	00 20 41.61	+59 16 24.8	22.75	0.36	99.99	0.56	0.46	WN4		[MAC92] 21	2,4

Note. — Notes—Units of right ascension are hours, minutes, and seconds, and units of declination are degrees, arcminutes, and arcseconds. Note that an entry of “99.999” denotes no measurement.

<sup>a</sup> “M” denotes multiple cross-identifications due to crowding.

References. — For spectral types: (1) Massey et al. 1992; (2) Massey & Armandroff 1995; (3) Massey & Holmes 2002; (4) Crowther et al. 2003.

Table 19. NGC 6822 Members Confirmed by Spectroscopy

LGS	$\alpha_{2000}$	$\delta_{2000}$	$V$	$B - V$	$U - B$	$V - R$	$R - I$	Sp. Type	Notes <sup>a</sup>	Cross-ID	Ref.
J194422.24-144342.4	19 44 22.24	-14 43 42.4	17.33	1.51	1.51	0.94	...	RSG		N6822a-96 <sup>d</sup>	6
J194431.99-144409.1	19 44 31.99	-14 44 09.1	19.69	-0.18	-0.76	0.28	0.16	WN	M	N6822-WR3 <sup>b</sup>	2
J194434.21-144219.9	19 44 34.21	-14 42 19.9	17.75	0.40	-1.09	0.07	0.02	O9.5 I	M	N6822ob3-7=F9 <sup>c,g</sup>	1
J194437.97-145106.2	19 44 37.97	-14 51 06.2	19.83	0.01	-0.76	0.12	0.10	WN		N6822-WR4 <sup>b</sup>	2
J194501.60-145440.0	19 45 01.60	-14 54 40.0	16.88	0.28	-0.59	0.19	0.21	B8-A0: I		E141 <sup>c</sup>	5
J194448.11-144518.1	19 44 48.11	-14 45 18.1	18.48	2.03	2.08	1.07	0.97	RSG		N6822b-356 <sup>d</sup>	6
J194448.65-145025.9	19 44 48.65	-14 50 25.9	18.85	0.86	0.16	0.55	0.53	Emission		C72 <sup>c</sup>	5
J194449.03-144526.9	19 44 49.03	-14 45 26.9	17.54	0.12	-0.74	0.11	0.08	EarlyB		N6822ob7-15=B17 <sup>c,e</sup>	1
J194449.31-144404.1	19 44 49.31	-14 44 04.1	18.20	0.09	-0.79	0.13	0.16	B0 Ia		N6822ob6-16	3
J194449.36-144539.8	19 44 49.36	-14 45 39.8	19.72	0.28	-0.63	0.29	0.40	WN		N6822-WR5 <sup>b</sup>	2
J194449.96-144333.5	19 44 49.96	-14 43 33.5	18.07	2.21	2.09	1.29	...	M2.5 I		N6822b-395 <sup>d</sup>	6
J194450.21-144253.6	19 44 50.21	-14 42 53.6	16.93	0.23	-0.71	0.15	0.14	B1.5 III		N6822ob8F-2=D14 <sup>c,f</sup>	1
J194451.10-144355.4	19 44 51.10	-14 43 55.4	18.81	1.98	1.49	1.40	1.64	M2.5 I/M1 I		N6822b-434=V12 <sup>d</sup>	6, 5
J194451.18-144919.8	19 44 51.18	-14 49 19.8	17.50	0.23	-0.44	0.20	0.17	B0-1 Ia		A66 <sup>c</sup>	5
J194451.53-144429.5	19 44 51.53	-14 44 29.5	18.70	1.87	1.31	1.03	0.94	K0-3 I		N6822b-395 <sup>d</sup>	6
J194451.67-144351.8	19 44 51.67	-14 43 51.8	17.70	2.03	0.15	1.13	...	K5 I/M0-1 I		N6822b-1133=C26 <sup>d</sup>	6, 5
J194452.28-145220.6	19 44 52.28	-14 52 20.6	16.45	0.36	-0.16	0.20	0.21	B1 I		C74 <sup>c</sup>	5
J194453.25-144640.3	19 44 53.25	-14 46 40.3	17.39	0.32	-0.35	0.21	0.26	A3 Ia		A13=CW185 <sup>c</sup>	4
J194453.96-144424.3	19 44 53.96	-14 44 24.3	18.19	2.01	1.94	1.04	...	RSG		N6822b-1134 <sup>d</sup>	6
J194454.54-145127.1	19 44 54.54	-14 51 27.1	17.05	2.25	2.15	1.19	...	M0-1 I		C79 <sup>c</sup>	5
J194454.81-144347.8	19 44 54.81	-14 43 47.8	18.05	2.24	-0.30	1.28	1.30	cM/RSG		N6822b-554=V14 <sup>d</sup>	5, 6
J194455.08-145213.1	19 44 55.08	-14 52 13.1	15.99	0.70	0.02	0.27	...	B5 Ia		C84 <sup>c</sup>	5
J194455.27-144631.6	19 44 55.27	-14 46 31.6	18.96	0.19	-0.39	0.30	0.33	Early BI	M	N66822ob7F-40	1
J194455.47-144930.0	19 44 55.47	-14 49 30.0	17.72	0.27	-0.28	0.20	0.23	B1-2 I		A73 <sup>c</sup>	5
J194455.70-145155.4	19 44 55.70	-14 51 55.4	16.91	2.20	1.99	1.17	...	M1-2 I		V18	5
J194456.19-144503.0	19 44 56.19	-14 45 03.0	16.68	0.35	-0.73	0.18	0.16	OB		B1 <sup>c</sup>	5
J194456.32-144612.1	19 44 56.32	-14 46 12.1	17.22	0.80	-1.04	0.19	0.22	A2 Ia		A101=CW173 <sup>c</sup>	4
J194457.31-144920.2	19 44 57.31	-14 49 20.2	17.41	2.28	-0.04	1.21	...	M1 I		V19	5
J194457.44-144345.0	19 44 57.44	-14 43 45.0	19.43	-0.05	-0.73	0.00	-0.02	Of:		N6822ob9-20A	1
J194458.31-144446.9	19 44 58.31	-14 44 46.9	17.89	2.11	1.34	1.18	1.15	cM/RSG	M	N6822b-684=V15 <sup>d</sup>	5, 6
J194459.78-144857.6	19 44 59.78	-14 48 57.6	17.94	0.06	-0.36	0.10	0.07	B5 I		A165 <sup>c</sup>	5
J194459.86-144515.4	19 44 59.86	-14 45 15.4	16.93	2.00	1.81	1.00	...	M0 I/RSG	M	N6822b-210=B110 <sup>d</sup>	5, 6
J194500.31-144434.9	19 45 00.31	-14 44 34.9	18.46	0.06	-0.66	0.09	0.06	B2 Ia		N6822ob11-8	3
J194500.42-144823.1	19 45 00.42	-14 48 23.1	17.35	0.31	-0.42	0.34	0.47	B5 I	M	A153 <sup>c</sup>	5
J194501.91-144732.2	19 45 01.91	-14 47 32.2	17.55	1.01	0.57	0.61	0.57	RSG		N6822c-108 <sup>d</sup>	6
J194505.25-144312.4	19 45 05.25	-14 43 12.4	18.20	0.30	-0.91	-0.23	-0.45	Early O	M	N6822ob13-9	1
J194513.26-144508.0	19 45 13.26	-14 45 08.0	18.02	-0.09	-0.69	0.01	-0.07	Early B		N6822ob15-9	1
J194513.50-144512.9	19 45 13.50	-14 45 12.9	18.96	-0.17	-0.54	0.16	0.04	WNE	M	N6822-WR12	2

Note. — Notes—Units of right ascension are hours, minutes, and seconds, and units of declination are degrees, arcminutes, and arcseconds. Note that an entry of “99.999” denotes no measurement.

<sup>a</sup> “M” denotes multiple.

<sup>b</sup> For the WR stars, we have retained the nomenclature of Massey & Johnson 1998; the CDS lists these stars as “[AM85] N”.

<sup>c</sup> Designations from Kayser 1966 (“A” refers to her inner-most field), some of which are cross referenced to Wilson 1992 (“CW”, following Massey et al. 1995a).

<sup>d</sup> For the RSGs, we have used the designations of Massey (1998b), cross referenced when possible to Kayser 1966.

<sup>e</sup> Classified as “A0 Ia” by Humphreys 1980a.

<sup>f</sup> Classified as “B5-8 I” by Humphreys 1980a.

<sup>g</sup> Classified as “B1-2 I” by Humphreys 1980a.

References. — For spectral types: (1) Massey et al. 1995a; (2) Massey & Johnson 1998; (3) Muschelok et al. 1999; (4) Venn et al. 2001; (5) Humphreys 1980a; (6) Massey 1998b.

Table 20. WLM Members Confirmed by Spectroscopy

LGS	$\alpha_{2000}$	$\delta_{2000}$	$V$	$B - V$	$U - B$	$V - R$	$R - I$	Sp. Type	Notes <sup>a</sup>	Cross-ID <sup>b</sup>	Ref.
J000153.19-152729.1	00 01 53.19	-15 27 29.1	19.01	-0.15	-0.89	-0.05	-0.10	B2II		B10=SC27	1
J000153.22-152839.5	00 01 53.22	-15 28 39.5	17.97	0.00	-0.67	0.03	0.01	B9Ia		A12=SC22	1
J000153.33-152851.9	00 01 53.33	-15 28 51.9	19.88	-0.19	-0.75	-0.07	-0.10	B2.5Ib		A13=SC21	1
J000153.63-152829.8	00 01 53.63	-15 28 29.8	18.87	-0.15	-0.85	-0.05	-0.10	B1Ia		B13=SC23	1
J000154.06-152745.4	00 01 54.06	-15 27 45.4	19.32	-0.17	-0.87	-0.05	-0.09	B0Iab		A10=SC26	1
J000155.03-152659.7	00 01 55.03	-15 26 59.7	19.55	-0.10	-0.66	-0.02	-0.07	B3Ib		A8=SC55	1
J000155.69-152449.0	00 01 55.69	-15 24 49.0	20.48	-0.11	-0.59	0.01	-0.06	B5II		B3=SC58	1
J000156.16-152624.5	00 01 56.16	-15 26 24.5	19.79	0.22	0.01	0.18	0.20	A7Ib		A6=SC51	1
J000156.34-152758.3	00 01 56.34	-15 27 58.3	19.77	-0.02	-0.49	0.08	0.08	A0Iab		B11	1
J000156.36-152606.7	00 01 56.36	-15 26 06.7	19.97	0.09	-0.08	0.09	0.14	A2II		B6=SC52	1
J000156.45-152901.6	00 01 56.45	-15 29 01.6	19.90	-0.04	-0.39	0.01	0.01	A0Ib		B14	1
J000156.62-152501.5	00 01 56.62	-15 25 01.5	21.09	1.09	-0.05	0.62	0.54	G0I		A3	1
J000156.75-152636.6	00 01 56.75	-15 26 36.6	20.27	0.11	-0.35	0.15	0.10	A3II		B8	1
J000157.17-152614.3	00 01 57.17	-15 26 14.3	20.31	0.14	-0.02	0.15	0.17	A3II		B7	1
J000157.20-152718.0	00 01 57.20	-15 27 18.0	18.39	0.20	-1.25	-0.03	-0.06	B1.5Ia		A9=SC35	1
J000157.89-153013.1	00 01 57.89	-15 30 13.1	18.38	0.20	-0.73	0.06	0.05	A2Ia		A16=SC16	1
J000158.12-152648.5	00 01 58.12	-15 26 48.5	19.66	-0.09	-0.97	-0.05	-0.11	B1.5Ia		A7=SC37	1
J000158.46-152433.8	00 01 58.46	-15 24 33.8	20.88	1.56	100.00	0.83	0.75	G5I		A1	1
J000158.73-153001.5	00 01 58.73	-15 30 01.5	20.03	-0.02	-0.32	0.05	0.04	comp	M	B16=SC12	1
J000159.04-152442.8	00 01 59.04	-15 24 42.8	20.14	-0.01	-0.23	0.05	0.03	A0II		A2=SC68	1
J000159.41-153046.7	00 01 59.41	-15 30 46.7	21.13	-0.05	-0.93	0.10	0.08	comp		B18	1
J000159.56-152926.1	00 01 59.56	-15 29 26.1	18.37	0.09	-0.16	0.07	0.12	A2II		A14=SC15	1
J000159.61-153059.9	00 01 59.61	-15 30 59.9	18.98	1.78	1.55	0.91	0.82	G2I		A18=SC4	1
J000159.88-152528.3	00 01 59.88	-15 25 28.3	20.89	0.26	-0.01	0.22	0.19	A5II		B4	1
J000159.95-152819.0	00 01 59.95	-15 28 19.0	18.38	-0.11	-1.04	-0.07	-0.12	O9.7Ia		A11=SC30	1
J000200.02-152545.0	00 02 00.02	-15 25 45.0	20.85	-0.03	-0.37	0.02	-0.04	A0II		B5	1
J000200.03-152930.9	00 02 00.03	-15 29 30.9	20.27	0.19	0.01	0.16	0.19	A5II		B15	1
J000200.19-153014.1	00 02 00.19	-15 30 14.1	20.19	-0.03	-0.52	0.06	0.04	comp		B17	1
J000200.48-153108.1	00 02 00.48	-15 31 08.1	19.74	-0.16	-0.73	-0.09	-0.09	B2Ib		B19	1
J000200.52-152951.8	00 02 00.52	-15 29 51.8	20.25	-0.28	-0.98	-0.12	-0.15	O7V((f))		A15=SC14	1
J000200.62-152829.8	00 02 00.62	-15 28 29.8	18.76	0.08	-0.12	0.09	0.61	A2II		B12=SC31	1
J000200.81-153024.8	00 02 00.81	-15 30 24.8	19.31	-0.11	-0.59	-0.03	0.45	B5Ib		A17=SC9	1
J000200.81-153115.7	00 02 00.81	-15 31 15.7	18.69	1.78	0.77	0.91	0.34	G2I		A19=SC6	1
J000201.57-152527.0	00 02 01.57	-15 25 27.0	20.18	0.02	-0.17	0.04	0.06	A2II		A4	1
J000201.91-152725.2	00 02 01.91	-15 27 25.2	19.77	0.01	-0.26	0.04	0.07	A0II		B9=SC42	1
J000203.31-152552.6	00 02 03.31	-15 25 52.6	19.41	-0.12	-0.58	-0.02	-0.08	B8Iab		A5=SC45	1
J000204.38-152446.5	00 02 04.38	-15 24 46.5	20.51	-0.10	-0.47	-0.02	-0.04	A2Ia		B2	1
J000205.15-152422.9	00 02 05.15	-15 24 22.9	20.96	0.14	0.05	0.17	0.16	A2II		B1	1

Note. — Notes—Units of right ascension are hours, minutes, and seconds, and units of declination are degrees, arcminutes, and arcseconds. Note that an entry of “99.999” denotes no measurement.

<sup>a</sup>“M” denotes multiple.

<sup>b</sup>Designations “A” and “B” from Bresolin et al 2006; “SC” from Sandage & Carlson 1985b.

References. — For spectral types: (1) Bresolin et al. 2006.